

## Recent progress in metal–organic polymers as promising electrodes for lithium/sodium rechargeable batteries

Wu, Zhenzhen; Xie, Jian; Xu, Zhichuan Jason; Zhang, Shanqing; Zhang, Qichun

2019

Wu, Z., Xie, J., Xu, Z. J., Zhang, S., & Zhang, Q. (2019). Recent progress in metal–organic polymers as promising electrodes for lithium/sodium rechargeable batteries. *Journal of Materials Chemistry A*, 7(9), 4259–4290. doi:10.1039/C8TA11994E

<https://hdl.handle.net/10356/144104>

<https://doi.org/10.1039/C8TA11994E>

---

© 2019 Royal Society of Chemistry. All rights reserved. This paper was published in *Journal of Materials Chemistry A* and is made available with permission of Royal Society of Chemistry.

*Downloaded on 28 Aug 2022 03:17:30 SGT*

# Recent Progress in Metal-Organic Polymers as Promising Electrodes for Lithium/Sodium Rechargeable Batteries

Zhenzhen Wu,<sup>†ab</sup> Jian Xie,<sup>†a</sup> Zhichuan J. Xu,<sup>a</sup> Shanqing Zhang,<sup>\*b</sup> Qichun Zhang<sup>\*a</sup>

Received 00th January 20xx,  
Accepted 00th January 20xx

DOI: 10.1039/x0xx00000x

www.rsc.org/

Metal organic polymers (MOPs), including metal coordination polymers (CPs, one-dimensional), metal organic frameworks (MOFs, two-/three-dimensional), Prussian blue (PB) and Prussian blue analogues (PBAs), have recently emerged as promising electrochemically-active materials for energy storages and conversion systems. Due to the tunability of their composition and the structural versatility, diverse electrochemical behaviors for multi-electron reactions, fast-ion diffusion, and small volume change of electrodes could be achieved upon charging and discharging. Because of these superiorities, MOPs are considered as effective substitutes for future advanced energy storage systems. Here, we summarize the recent progress in pristine MOPs as electrode candidates for rechargeable lithium and sodium ion batteries. The working mechanisms and strategies for enhancing the electrochemical performance in related advanced electrochemical energy storage (EES) applications are also highlighted in this review.

## 1. Introduction

The rapid advances of electrochemical energy storage (EES) techniques originate from the contradiction between the intermittent/fluctuating supply of nature energy and continually-growing demand for mobile power consumption.<sup>1</sup> The demand of high energy-density systems triggers the boom of portable EES devices, including secondary batteries (e.g. Li-ion, Na-ion, Li-S, Na-S, etc.) and supercapacitors. For this reason, a large amount of available and sustainable electrode materials have been developed.<sup>2-5</sup> Among all fascinating battery systems, lithium-ion battery (LIB) and sodium-ion battery (SIB) are the most promising devices due to their superior energy/rate ability, ultra-long cycling stability, zero memory effect, and low price.<sup>6, 7</sup> In recent year, with the deep research of LIB and SIB, there are various electrode materials are found and included in energy storage field, such as 2D materials and metal oxide composites.<sup>8-12</sup> As one family member of candidates for energy-storage materials, coordination polymers (CPs, one-dimensional) and metal-organic frameworks (MOFs two-/three-dimensional) have been confirmed as potential electrode materials owing to their several advantages: (1) the rich variety of choices (>20,000 species); (2) the adjustable pore spaces; (3) robust and tunable framework structures; (4) well-organized open channels; (5) high chemical/thermal stability; and (6) multi-electron reactions (Fig. 1).<sup>1, 13-22</sup>

Several terminology guidelines in this review need to be distinguished for clear understanding of the topics. The term of Metal organic polymers (MOPs) is used to describe the

materials with metal node centers bridged with more than one ligands, and this binding (or coordination interaction) are extended to an infinite array with one-/two-/three- dimensional structures.<sup>23-26</sup> MOPs consist of CPs, MOFs, Prussian blue (PB), and Prussian blue analogues (PBAs). Although PB was firstly found in 18<sup>th</sup> century with the general formula of  $\text{Fe}_4[\text{Fe}(\text{CN})_6]_3 \cdot x\text{H}_2\text{O}$ , its application in rechargeable batteries is less developed comparing to CPs and MOFs.

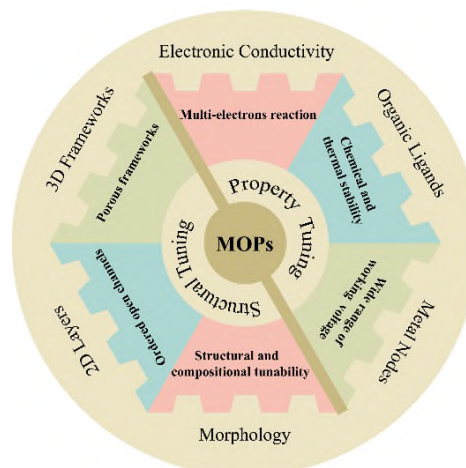


**Fig.1** Brief illustration of material features and modification strategies of redox-active metal organic polymers for energy storage.

In recent years, enormous efforts have been input to molecular devising, structure layout,<sup>27, 28</sup> experimental synthesis<sup>29, 30</sup> of MOPs, and their advanced applications. Elaborate selections of various functional groups for organic ligands, different valence or species for metal clusters, and smart pores or building cells can yield versatile ways for the

<sup>a</sup> School of Materials Science and Engineering, Nanyang Technological University, Singapore, 639798, Singapore. E-mail: qc Zhang@ntu.edu.sg.

<sup>b</sup> Centre for Clean Environment and Energy, School of Environment and Science, Gold Coast Campus, Griffith University, QLD 4222, Australia. E-mail: s.zhang@griffith.edu.au

<sup>†</sup> Both authors have equal contribution to this paper.

utilization of MOPs materials. They can be used not only on traditional gas capture<sup>31-33</sup> and metal ions separation<sup>34-37</sup> but also on bio-mass express,<sup>38</sup> chemical sensor,<sup>39-42</sup> optical/electric catalysts<sup>43-49</sup> and EES-related cells.<sup>50-55</sup> Due to the diversity of porous frameworks and multiformity of chemical elements, pristine MOPs can be used beyond the field of battery, from separator/membrane,<sup>56-59</sup> solid/liquid electrolyte,<sup>60-62</sup> host for redox-active materials (Si,<sup>63</sup> sulfur,<sup>64-67</sup> metal oxides,<sup>68</sup> metal particles<sup>69</sup>), to electrochemically-active electrode materials. Building on our previous works on metal chalcogenide crystals as active materials in Li-ion batteries,<sup>70, 71</sup> the successful experience to overcome the issues of the bulk pulverization and volume expansion would help us to design MOPs with high specific capacity and long cycles. In fact, we are actively working on these materials and several primary results have been achieved.

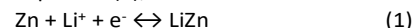
This review will comprehensively focus on the exploration of MOPs, particularly CPs, MOFs, PB and their analogous (PBAs), as redox-active electrode materials in rechargeable lithium-ion batteries and sodium-ion batteries. Although tremendous inorganic porous materials with well-designed structures, such as nanostructured metal-based compounds ( $M_xS_y$ ,  $M_xO_y$ ,  $M_xO_y/C$ ,  $M_xO_y/M$ )<sup>72-76</sup> and carbon nanomaterials (N-doped carbon, hollow or core-shell carbon)<sup>77-82</sup> derived from crystal MOPs precursors, have been widely discussed in recent reviews, our discussion will only cover pristine MOPs as lithium/sodium ion storage materials. Strictly speaking, instead of pure crystals, MOFs-derived compounds are similar to common nanomaterials without preserved topotactic crystallinity and distinctive nanoporous channels. From this perspective of view, here we begin with the discussion of general electrochemical mechanisms of MOPs electrodes, including the comparison of conversion-type, insertion-type, and a novel intercalation scheme – “bipolar charging”. The contributing factors that dominate the ion storage capacity, rate capability, and cycling stability are introduced with respect to whether metal clusters or organic moieties are involved into the redox-reactions or not. Then, to further improve the battery performance, we propose six strategies classified from recent progresses in pristine MOPs electrodes materials including: (1) the substitution and optimization of metal nodes; (2) the tuning and functionalization of bridging ligands; (3) the control and enhancement of electronic conductivity; (4) high operation voltage realization-cathodes applications; (5) PBAs-based electrodes materials; and (6) other approaches (the tunability of particles size and pores type, multifarious morphology and so on). Finally, apart from LIB/SIB, we promote pristine MOPs to other cation-based batteries, such as potassium ion battery, zinc ions battery, and magnesium ion battery. By summarizing and identifying recent evolutions on intact MOPs for EES-related applications, we expect to provide some aid for further investigation on pristine MOPs as battery electrodes.

## 2. Redox-Reaction Chemistries of Pristine Metal Organic Polymers

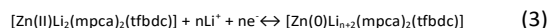
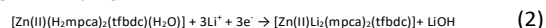
Li-ion batteries (LIBs) are commonly referred to “rocking-chair” batteries, because they can provide chemical energy via a reversible “rocking” of  $Li^+$  back and forth between the positive and negative electrodes during the charge/discharge process.<sup>83</sup> Specifically, the storage and supply of chemical energy from an electrode is achieved by the reversible acceptance and the release of  $Li^+$  between the electrode and electrolyte, which can be mediated through  $Li^+$  intercalation or the breaking/reforming of chemical bonds with an accompanying movement of electrons.<sup>17</sup> Similarly, it has been proposed that MOPs-based electrodes could store and deliver electrochemical energy through two specific mechanisms: conversion type (usually following an alloying/de-alloying process) and insertion-type.

### 2.1 Conversion-Type Reaction

When MOPs undergo conversion-type reactions, the central metal ions are usually reduced into metallic state or lithium-containing alloys. Due to the huge transition of the chemical composition during charge/discharge, the entire MOPs framework structures inevitably collapse.<sup>84</sup> Chen et al. firstly used the conversion principle to explain the lithium storage mechanism of a MOF-177 (or  $Zn_4O(BTB)_2$ ) anode, with a theoretical capacity of 190 mAh g<sup>-1</sup>.<sup>85</sup> During the first step of lithiation process, MOF-177 is reduced into metallic Zn and  $Li_2O$ , which is accompanied with the destruction of the integrated framework (Fig. 2a-b). Then, guest molecules such as N,N-diethylformamide (DEF) and  $H_2O$  react with  $Li^+$  to form  $Li_2(DEF)$  and  $LiOH$ . The final step is a reversible alloying/de-alloying reaction, as shown in equation (1);



The proposed mechanism delivers a specific capacity of ~ 100 mAh g<sup>-1</sup> after the first cycle. In contrast to the poor cyclability of MOF-177,  $Zn_3(HCOO)_6$  with a simple ligand shows stable cyclic performance over many cycles via a reversible conversion reaction.<sup>86</sup> An invariable specific capacity of 560 mAh g<sup>-1</sup> is obtained after 60 cycles at 60 mA g<sup>-1</sup> between 0.005V and 3.0V (Vs.  $Li/Li^+$ ). Upon  $Li^+$  incorporation into  $Zn_3(HCOO)_6$  during the discharging process, the metal-formate scaffold is reversibly converted into lithium formate and metallic Zn, instead of forming the irreversible side-product  $Li_2O$ . The subsequent Zn/ $LiZn$  alloying reaction further maintains a stable lithium storage. Besides MOFs, some metal-based coordination polymers (CPs) also present the similar conversion scheme. Zn-ODCP, with the formula of  $Zn(H_2mpca)_2(tfbdc)(H_2O)$  ( $H_2mpca$  = 3-Methylpyrazole-4-carboxylic acid;  $H_2tfbdc$  = Tetrafluorobenzene-1,4-dicarboxylic acid), was firstly applied as an anode to accommodate Li (up to 26 mol of Li).<sup>87</sup> This Zn-based CP still expresses reversible conversion and alloying/dealloying reactions:



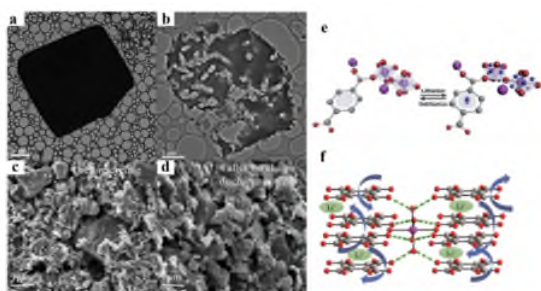


**Fig. 2** TEM images of the MOF-177: (a) primary sample before electrochemical tests; (b) destructive structure after 1<sup>st</sup> discharge. Reproduced with permission from ref.85. Copyright 2006 Elsevier. SEM images of [Ni(NA)<sub>n</sub>]: (c) before, and (d) after charge-discharge. Reproduced with permission from ref.94. Copyright 2018 American Chemical Society. (e) The proposed Li-ions insertion sites at carboxylate groups and the benzene rings (purple-Co, claret-red-O, gray-C, blue-Li). Reproduced from ref.95. with permission from The Royal Society of Chemistry. (f) Possible scheme of Li ions transportation in layer structured materials (purple-Co, red-O, green-Li). Reproduced with permission from ref.96. Copyright 2018 Elsevier.

During the first cycle, the coordinated H<sub>2</sub>O and decomposed electrolyte produce the irreversible formation of LiOH, which causes the electrode to present an initial coulombic efficiency as low as 39.5%. However, a specific capacity of 342 mAh g<sup>-1</sup> is delivered at the second cycle, and 300 mAh g<sup>-1</sup> remains at the 50<sup>th</sup>. The good cycling performance of this Zn-based CP comes from (1) multi-redox active sites including Zn(II) and conjugated carboxylates from mpca and tfbdc ligands; (2) flexible 1D chains, which provide shorter Li ions diffusion space; and (3) the reversible transformation and regeneration of CP structure. Additionally, similar battery reaction principles have been used to explain the case of Co<sub>3</sub>(HCOO)<sub>6</sub>,<sup>86</sup> Mn-LCP (Mn(tfbdc)(4,4'-bpy)(H<sub>2</sub>O)<sub>2</sub>),<sup>88</sup> Cu-BDC [Cu<sub>2</sub>(C<sub>8</sub>H<sub>4</sub>O<sub>4</sub>)<sub>4</sub>]<sub>n</sub>,<sup>89</sup> Ni-Me<sub>4</sub>bpz ([H<sub>2</sub>Me<sub>4</sub>bpz = 3,3',5,5'-tetramethyl-4,4'-bipyrazole]),<sup>90</sup> Zn-LMOF (Zn(4,4'-bpy)(tfbdc)(H<sub>2</sub>O)<sub>2</sub>),<sup>91</sup> Co-LCP (Co(tfbdc)(4,40-bpy)(H<sub>2</sub>O)<sub>2</sub>),<sup>92</sup> and CoCOP (polycarboxylate-Co coordination polymer).<sup>93</sup>

## 2.2 Insertion-Type Reaction

Even though several modifications have been suggested to overcome the limited cycle life for the conversion-type MOPs, their limited cyclability still cannot satisfy the existing energy storage devices because of the obvious degradation of structures and compositions. As such, the insertion-type MOPs have gained more attention as their structures tend to be maintained after Li<sup>+</sup> insertion/extraction reactions, which can provide stable and quick ion diffusion channels.<sup>15</sup> During the lithiation/delithiation process, metal cations such as Li<sup>+</sup>/Na<sup>+</sup> are transferred between the electrolyte and the pores or the framework of MOPs electrodes. In addition, pristine MOPs possess multi-redox active sites at the inorganic metal hubs and organic bridging ligands, leading to a high theoretical specific capacity and rate capability. However, different coordination surroundings, including the valence or kind of metal nodes and diverse groups of organic linkers, may influence the active-redox reaction sites.<sup>97</sup> Depending on the functional components

that provide redox active sites, MOPs can be classified into three different classes: redox active inorganic metal nodes-dominant, redox active organic bridging ligands-dominant, and both redox active inorganic/organic moieties.

### 2.2.1 Insertion Type: Redox Active Inorganic Metal Nodes-Dominant.

Li storage can be achieved by the redox couples of metal nodes, such as Fe<sup>3+</sup>/Fe<sup>2+</sup>, Ni<sup>3+</sup>/Ni<sup>2+</sup>, V<sup>5+</sup>/V<sup>4+</sup>, V<sup>4+</sup>/V<sup>3+</sup> and so on. Once lithium ions are inserted into the frameworks, metal ions will be reduced into lower oxidation states to balance the charge in the whole electrode. However, the number of electrons that the metal-ion redox couples can offer is much smaller than that of organic ligands. Thus, a limited theoretical gravimetric energy density is inevitable for redox active metal nodes-dominant MOPs. Since Tarascon et al. proposed the lithium storage possibility of MIL-53 (Fe) Fe<sup>III</sup>(OH)<sub>0.8</sub>Fo<sub>0.2</sub>(O<sub>2</sub>CC<sub>6</sub>H<sub>4</sub>CO<sub>2</sub>), redox active Fe-based MOFs via the Fe<sup>3+</sup>/Fe<sup>2+</sup> couples have gradually attracted considerable interests. Examples including MIL-101(Fe) and MIL-100 (Fe) have been thoroughly investigated.<sup>98-104</sup> MIL-53 (Fe) exhibits a gravimetric capacity of 75 mAh g<sup>-1</sup> and a volumetric capacity of 140 mAh L<sup>-1</sup> when cycled at 0.025C in the voltage range of 1.5-3.5V (Vs. Li/Li<sup>+</sup>). During the charge/discharge process, 0.6 Li<sup>+</sup> ions are taken up/removed per unit formula, accompanied by the Fe<sup>3+</sup>/Fe<sup>2+</sup> redox couple. Similar Fe<sup>3+</sup>/Fe<sup>2+</sup> mixed valence states also occur during lithiation/delithiation in the MIL-101(Fe) electrode, delivering 0.2 Li<sup>+</sup> per Fe after 30 cycles at 0.1 C between 2.0-3.5V. But the oxidation of Fe<sup>2+</sup> to Fe<sup>3+</sup> is irreversible after many cycles, due to higher energy is required for further insertion of Li<sup>+</sup> in MIL-101(Fe) framework. Additionally, the lithium ion storage mechanism of MIL-47 (V) [V<sup>IV</sup>(O)(bdc)],<sup>105</sup> KLi[(VO)<sub>2</sub>(HPO<sub>4</sub>)<sub>2</sub>(C<sub>2</sub>O<sub>4</sub>)],<sup>106</sup> Li<sub>2</sub>(VO)<sub>2</sub>(HPO<sub>4</sub>)<sub>2</sub>(C<sub>2</sub>O<sub>4</sub>),<sup>107</sup> or Ni (TA) (TA= trimesic acid),<sup>108</sup> can also be explained by the same redox active metal nodes-dominant scheme.

### 2.2.2 Insertion Type: Redox-Active Organic Bridging Ligands-Dominant.

The versatility and tunability of redox active functional groups at organic linkers make them desirable to realize multi-electrons reactions. Like many organic electrode materials, such as conjugated carbonyl compounds and conducting polymers, the electrochemical active sites of bridging linkers are mainly located at oxygen atom-based groups (-COO-, -C=O), nitrogen atom-based groups (imidazole, pyridine, amine group), and aromatic ring containing delocalized  $\pi$  electrons clouds.

The synergistic lithium storage effect between carboxyl and benzene rings has shown great success in MOPs, as showing in Fig. 2e-f, on the basis of the linkers of 1,3,5-benzenetricarboxylate (BTC),<sup>109-112</sup> 1,4-benzenedicarboxylic acid (BDC),<sup>95, 113-115</sup> 1,2,4,5-benzenetetracarboxylic acid,<sup>116</sup> 2,5-dihydroxyterephthalic acid,<sup>117</sup> 1,4-naphthalene dicarboxylate (NDC),<sup>118,119</sup> and so on. The presence of conjugated carboxylates, which show weak withdrawing electron effects

and have strong  $\pi$  -  $\pi$  interactions with the aromatic core, can lead to a stable framework of MOPs.<sup>111, 112</sup> Moreover, the high theoretic capacity and rate ability can be obtained through the redox coordination of  $\text{COO}^-$  and  $\text{Li}^+$  as well as the accommodation of  $\text{Li}^+$  at each benzene ring (maximum up to  $6\text{Li}^+$  per aromatic ring) with enhanced ionic conductivity.<sup>120</sup> Mahanty et al. prepared Mn-BTC MOFs (Mn-1,3,5-benzenetricarboxylate) as an anode for LIBs, which expressed a high specific capacity of  $694\text{ mAh g}^{-1}$  at the current density of  $103\text{ mA g}^{-1}$  between 0.01 and 2.0V (vs.  $\text{Li/Li}^+$ ) with a 83% capacity retention at the 100<sup>th</sup> cycles.<sup>112</sup> Even when tested at a higher current density of about  $1.0\text{ A g}^{-1}$ , the Mn-1,3,5-benzenetricarboxylate-based electrode displays a stable capacity of around  $400\text{ mAh g}^{-1}$  after few initial cycling and demonstrates a  $\sim 100\%$  capacity retention after 100 cycles. The same ligands were used to synthesize Cu-BTC MOFs,  $[\text{Cu}_3(1,3,5\text{-benzenetricarboxylate})_2]$ , an anode for LIBs.<sup>111</sup> A specific capacity of  $\sim 474\text{ mAh g}^{-1}$  is obtained at a high current density of  $\sim 383\text{ mA g}^{-1}$ , and a nearly 100% capacity retention is maintained after 50 cycles. Hu et al. applied Co-BDC MOFs as anode materials for storing lithium ions.<sup>114</sup> When it is evaluated at the potential windows of 0.01-3.0V (vs.  $\text{Li/Li}^+$ ) at  $200\text{ mA g}^{-1}$ , the discharge capacity of 100<sup>th</sup> cycle exhibits  $1090.2\text{ mAh g}^{-1}$ , which equals to 70.7% of the capacity during the first cycle. Moreover, when increasing the current density to  $500\text{ mA g}^{-1}$  and  $1\text{ A g}^{-1}$ , Co-BDC still can retain the discharge capacity of  $795\text{ mAh g}^{-1}$  and  $611\text{ mAh g}^{-1}$  until 200 cycles, respectively. Furthermore, the capacity only fades 3.2% after 200 cycles at  $500\text{ mA g}^{-1}$ . The strong interaction effect between  $\text{Li}^+/\text{Na}^+$  and electron-donating N atoms in heterocyclic ligands makes N-rich functional groups desirable for lithium/sodium intercalation. 3D coordination polymers, built with 5-hydroxynicotinic acid ( $\text{H}_2\text{NA}$ ), forming  $[\text{M}(\text{NA})_n]$  ( $\text{M} = \text{Co (II)}$  or  $\text{Ni (II)}$ ), show a high specific capacity of 618 and  $610\text{ mA h g}^{-1}$  at a current density of  $100\text{ mA g}^{-1}$  during the potential range of 0.01-3V (Vs.  $\text{Li/Li}^+$ ) at the 100<sup>th</sup> cycle, respectively.<sup>94</sup> Fig. 2c-d shows an example of  $[\text{Ni}(\text{NA})_n]_n$ , with a maintained morphology after the charge-discharge treatment. As for  $[\text{Co}(\text{NA})_n]$  anode, an excellent rate capability is evidenced by the capacity returning to  $742\text{ mAh g}^{-1}$  at  $50\text{ mA g}^{-1}$  after a successive rate test at  $50\text{ mA g}^{-1}$  ( $723\text{ mAh g}^{-1}$ ),  $100\text{ mA g}^{-1}$  ( $636\text{ mAh g}^{-1}$ ),  $200\text{ mA g}^{-1}$  ( $543\text{ mAh g}^{-1}$ ),  $500\text{ mA g}^{-1}$  ( $421\text{ mAh g}^{-1}$ ), and  $1000\text{ mA g}^{-1}$  ( $345\text{ mAh g}^{-1}$ ). XPS analysis demonstrates that with the redox innocent Co/Ni ions,  $\text{NA}^{2-}$  anions participate in Li attachment at carboxyl, hydroxy, nitrogen atom, and pyridine ring. In another case, Hu et al. fabricated Co-BDCN CPs through a one-pot synthesis, and the lithium ions are stored at the O and N atoms of amide and benzene ring.<sup>121</sup> A specific capacity of  $1132\text{ mAh g}^{-1}$  was achieved after the 100<sup>th</sup> cycle at  $100\text{ mA g}^{-1}$  between 0.01V and 3.0V (Vs.  $\text{Li/Li}^+$ ). Besides, imidazole-based MOFs also can undergo a lithium-ion binding process at the N atoms in organic ligands.<sup>122</sup> Zeolitic ZIF-8 and ZIF-67 have a stable capacity of 335.3 and  $311.6\text{ mAh g}^{-1}$  at 0.2C during 0.01-3.0 V (Vs.  $\text{Li/Li}^+$ ) after 70 cycles, respectively.<sup>123</sup> In addition, more organic ligands

with electrochemically-active N atoms, including abIM (2-aminobenzimidazole)<sup>122</sup> and HAB (hexaaminobenzene),<sup>97</sup> have been investigated and showed great potential as electrodes.

**2.2.3 Insertion Type: Both Redox-Active Inorganic/Organic Moieties.** Without the direct engagement of metal centers during the charge/discharge process, organic moieties (i.e.  $-\text{COO}^-$ ,  $-\text{NH}_2$ , benzene ring) can effectively complete the lithium insertion/de-insertion and provide multi-redox-electrons. Moreover, the intact metal centers that do not mediate electron transferring can play the role of stabilizing the whole framework. However, metal nodes will make gravimetric energy density lower because of its redox inactivity and high molecular weight. The review below aims to balance these counteracting points and gives good examples for further research.

u-CoOHTp, consisting of Co-terephthalate MOF, was found to have good Na-ion storage behavior ascribed to the introduction of oxygen vacancies at the unsaturated metal nodes. Oxygen vacancies were introduced via an expedient ultrasonic method and can enhance the ion- and charge-migration rates.<sup>124</sup> Ex-situ XAFS and sXAS analyses reveal that, during the discharge process,  $\text{Co}^{2+}$  is reduced into  $\text{Co}^0$  and carboxyl oxygen atoms is incorporated with  $\text{Na}^+$ . A mixed-phase of Co-MOF,  $\text{CoO}_x$ , and  $\text{Co}^0$  is produced at the charge process, however, their reversibility during the followed redox reaction process brings forth a stable and long cycling life. The discharge capacity of u-CoOHTp presents  $774\text{ mAh g}^{-1}$  on the 1<sup>st</sup> cycle and  $371\text{ mAh g}^{-1}$  on the 50<sup>th</sup> cycle at the test condition of 0.01-3.00 V (Vs.  $\text{Na/Na}^+$ ) and  $50\text{ mA g}^{-1}$ . When u-CoTDA ( $\text{H}_2\text{TDA} = 2,5\text{-thiophenedicarboxylic}$ ) is applied as an anode material for LIBs (0.01–3.00 V vs.  $\text{Li/Li}^+$ ), a high capacity of  $790\text{ mAh g}^{-1}$  could be maintained after 300 cycles at a current density of  $1\text{ A g}^{-1}$ , and  $548\text{ mAh g}^{-1}$  after 400 cycles at  $2\text{ A g}^{-1}$ .<sup>125</sup> Ex-situ CoK-edge XANES, OK-edge sXAS, and EPR observation conclude the reversible occurrence of  $\text{Co(II)/Co(0)}$  reaction and  $\text{Li}^+$  insertion/extraction on oxygen atoms at bridging ligands. Shen et al. reported Fe-BTC with Basolite F300-like structure, which delivered  $1021\text{ mAh g}^{-1}$  (100<sup>th</sup>,  $100\text{ mA g}^{-1}$ ),  $436\text{ mAh g}^{-1}$  (400<sup>th</sup>,  $500\text{ mA g}^{-1}$ ) and  $408\text{ mAh g}^{-1}$  (400<sup>th</sup>,  $1000\text{ mA g}^{-1}$ ), accompanied with  $\text{Fe}^{3+}/\text{Fe}^{2+}$  transformation and  $\text{Li}^+$  reversible accommodation/extraction on organic moieties.<sup>126</sup> Dong et al. activated  $-\text{COO}^-$  of MIL-53 (Fe) bridging linkers by modifying it with a high-conductivity RGO.<sup>127</sup> Besides, Cu-TCA ( $\text{H}_3\text{TCA} = \text{tricarboxytriphenyl amine}$ ) presents the redox properties both at the metal nodes of  $\text{Cu(II)/Cu(I)}$  and organic moieties of  $\text{N}^+/\text{N}$ .<sup>128</sup> Also, the coexistence of redox active metal centers and bridging ligands has been found in the samples of  $\text{Cu(2,7-AQDC)}$ ,<sup>129</sup>  $\text{Ni-NTC}$ ,<sup>130</sup> and  $\text{MIL-136(Ni, Co)}$ .<sup>131</sup>

### 2.3 Novel Insertion/Extraction Principle - "Bipolar Charging" Scheme

The ordered open channels and controllable pore space endow MOPs materials with unique "bipolar charging behavior" during

the charge/discharge process. For this reason, both cations (such as  $\text{Li}^+$ ,  $\text{Na}^+$ ) and anions (such as  $\text{PF}_6^-$  and  $\text{BF}_4^-$ ) can be

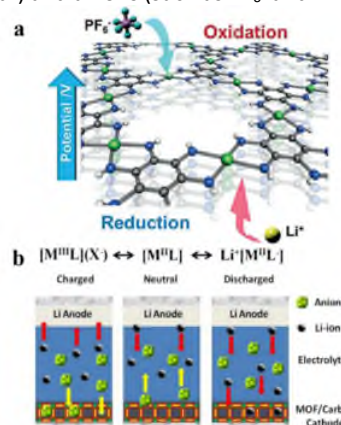


**Fig. 3** (a) Conceptual scheme of the redox reactions of NiDI accompanying with "bipolar charging" process. Reproduced with permission from ref.132. Copyright 2018 Wiley-VCH Verlag GmbH & Co. KGaA. (b) Schematic "bipolar charging" chemistry. Reproduced with permission from ref.133. Copyright 2016 American Chemical Society.

captured into the frameworks and contribute to the total capacity.<sup>15</sup> In a common case, anions ( $\text{PF}_6^-$ ) are taken up into the frameworks during the charge process, and cations ( $\text{Li}^+$ ) are impregnated during the discharge process, which is helpful to realize a less crowded ion transportation and fast-ion diffusion in solid state MOPs. Moreover, in the case of  $\text{Mn}_7(2,7\text{-AQDC})_6(2,6\text{-AQDC})(\text{DMA})_6$ , even though the ionic radius of  $\text{PF}_6^-$  is much larger than that of  $\text{Li}^+$ , these two ions exhibit comparable ion diffusion speeds. The novel and unique electrochemical mechanism of MOPs electrodes may offer a possible way to develop large migration ions, such as  $\text{Zn}^{2+}$ ,  $\text{Mg}^{2+}$ ,  $\text{Al}^{3+}$  and anions in new battery systems beyond  $\text{Li}^+$ .<sup>18</sup>

Nishihara et al. proposed a 2D conductive NiDI (bis(diimino)nickel) coordination framework, which was observed to provide energy storage by the uptake of both  $\text{PF}_6^-$  and  $\text{Li}^+$  (Fig. 3a).<sup>132</sup> The specific cation and anion movement and charge transition states are explained by: (1) the transformation between original neutral state (O) and positively oxidized state ( $\text{O}^+$ ) accompanied by the insertion/extraction of  $\text{PF}_6^-$ , corresponding to the anodic peak of 3.73 V and cathodic peak of 3.56 V in CV curves; (2) the transformation between original neutral state (O) and negatively reduced state ( $\text{O}^-$ ) accompanied by the insertion/desertion of  $\text{Li}^+$ , corresponding to the anodic/cathodic peak of  $\sim 3.21$  V. It is proposed that once redox active ions are inserted into the pores of NiDI, the charge of N atoms and Ni atoms in the framework will be re-arranged to stabilize the electronic structure. NiDI electrode shows a specific capacity of  $155 \text{ mAh g}^{-1}$  at  $10 \text{ mA g}^{-1}$ , and a stable capacity until the 300<sup>th</sup> cycle at the current density of  $250 \text{ mA g}^{-1}$ . Awaga et al. discovered that Mn-MOF, with the formula of  $\text{Mn}_7(2,7\text{-AQDC})_6(2,6\text{-AQDC})(\text{DMA})_6$  (AQDC = anthraquinone dicarboxylics, DMA = N, N-dimethylacetamide), offers the capacity based on its positive and negative forms, named "bipolar charging" scheme.<sup>133</sup> As shown in Fig. 3b, during the charge step,  $\text{Mn}^{2+}$  is oxidized into  $\text{Mn}^{3+}$  and bulk  $\text{PF}_6^-$  anions ( $\text{X}^-$ )

are inserted into the framework; while at the discharge process, the extraction of  $\text{PF}_6^-$  ions first happens, followed by the incorporation of  $\text{Li}^+$  and the reduction of ligands-anthraquinone groups (L). A capacity of  $205 \text{ mAh g}^{-1}$  was obtained at operation current of  $1 \text{ mA}$  within  $1.3\text{-}4.5\text{ V}$ , corresponding to the transformation of 2 electrons per AQDC ligand and 1 electron per Mn ions.

### 3. The Strategies for Enhancing the Performance of Electrodes

#### 3.1 Substitution and Optimization of Metal Nodes

The diverse organic ligands and multi-valent metal ions offer endless possibilities of chemical compositions and framework structures for MOPs materials, which bring forth many suitable choices in favour of enhancing battery performance.<sup>25</sup> There are many present forms of metal nodes in redox-MOPs, including mono-valent alkali metal ions, multi-valent transitional metal ions, mix-valent metal ions, and mixed-kinds metal ions, and so on.<sup>15, 16, 84, 91, 111, 118, 134-141</sup> Thus, it's necessary to discuss the possible choice of metal nodes in order to lay a foundation for future research. Considering that other sections mainly focus on the analysis of multi-valent metal nodes, the following paragraph will switch to those redox-MOPs characterized by (1) mono-valent metal ions and (2) mixed-kinds metal ions.

Different from the research of multi-valent transitional metal ions, less attention is paid to that of +1 value alkali ions ( $\text{Li}^+$ ,  $\text{Na}^+$ ,  $\text{K}^+$ ,  $\text{Rb}^+$ ,  $\text{Cs}^+$ ) in coordination polymers.  $[\text{Li}_2(\text{C}_6\text{H}_2\text{O}_4)]$  coordination polymer, bridged by Li-O bonds between 2,5-dihydroxy-1,4-benzoquinone ligands and lithium metal nodes, is prepared as a candidate for cathodes in LIBs as its C=O groups are good for reversible Li ion insertion/deinsertion at redox-active oxygen atoms.<sup>142</sup> When the test condition is set at  $100 \text{ mA g}^{-1}$  within  $1.5\text{-}3.5\text{ V}$  (Vs.  $\text{Li}/\text{Li}^+$ ), it presents an initial capacity of  $\sim 176 \text{ mAh g}^{-1}$  and up to  $137 \text{ mAh g}^{-1}$  after 10 cycles, which is much higher than that of  $90 \text{ mAh g}^{-1}$  delivered by the cathode based on ligand itself. Later, Devic et al. reported a series of 3D  $\text{M}_2(\text{TTF-TC})\text{H}_2$  coordination polymers derived from  $(\text{TTF-TC})\text{H}_4$  (= tetracarboxylic acid) and alkaline ions ( $\text{K}^+$ ,  $\text{Rb}^+$ ,  $\text{Cs}^+$ ), denoted as MIL-132(K), MIL-133(K or Rb), and MIL-134(Cs).<sup>143</sup> All of them show good thermal stability when exposed to  $150\text{-}200^\circ\text{C}$  air atmosphere. Interestingly,  $\text{K}(\text{TTF-TC}^+)\text{H}_2$ , based on the oxidized  $\text{TTF-TC}^+$  which is S-rich  $\pi$ -electron donors, exhibits an electronic conductivity of  $\sim 1 \text{ mS cm}^{-1}$  at room temperature and a charge capacity of about  $50\text{-}60 \text{ mAh g}^{-1}$  between 2V and 4V (Vs.  $\text{Li}/\text{Li}^+$ ) at  $10 \text{ mV s}^{-1}$  of solid-state CV. Chen et al. synthesized and studied a great deal of 3D alkali-cation coordination polymers bridged with  $\text{H}_2\text{OBA}$  (=4,4'-oxybisbenzoic acid), including  $[\text{Li}_2(\text{OBA})]$ ,  $[\text{Na}_2(\text{OBA})(\text{H}_2\text{O})]$ ,  $[\text{K}(\text{HOBA})]$ ,  $[\text{Rb}(\text{HOBA})]$ ,  $[\text{Cs}(\text{HOBA})]$ , with the merits of high thermal stability.<sup>144</sup> For  $\text{Li}_2(\text{OBA})$  CP anode ( $0.1\text{-}3\text{ V}$ ,  $1 \text{ Li}^+$  per  $10 \text{ h}$  vs.  $\text{Li}^0$ ), the 1<sup>st</sup> discharge capacity is  $106 \text{ mAh g}^{-1}$  and the 30<sup>th</sup> capacity remains at  $\sim 100 \text{ mAh g}^{-1}$ , showing a good cyclability. In summary, even though the research of alkali cations is not such a hot topic as that of transitional metal ions, they still provide more selectable

candidates for constructing redox-coordination polymers.<sup>138, 145-147</sup>

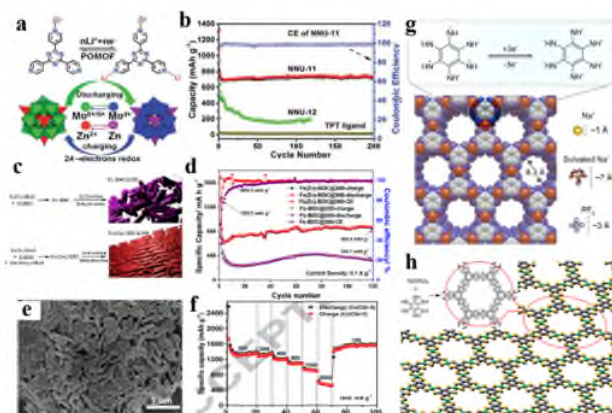


**Fig. 4** POM-based metal clusters: (a) Possible scheme of the reaction mechanism, (b) Cycling performance of NNU-11 at 50 mA g<sup>-1</sup> within 0.01-3.0 V (Vs. Li/Li<sup>+</sup>). Reproduced from ref.149. with permission from The Royal Society of Chemistry. Bimetal-based metal nodes: (c) Illustration of the synthesis of Fe-BDC@300 and Fe(Zn)-BDC@300, (d) Cycling performance of at 0.1 A g<sup>-1</sup> within 0.01-3.0 V (Vs. Li/Li<sup>+</sup>). Reproduced with permission from The Royal Society of Chemistry from ref.162. Electronic conductivity enhancement by adding carbon: (e) SEM of CoCGr-5 (5 wt% of carboxyl graphene), (f) Rate performance of CoCGr-5. Reproduced with permission from ref.163. Copyright 2017 Elsevier. HAB ligands: (g) Presentation of 3D calculated structure of two-dimensional Co<sup>II</sup>-HAB MOFs with 3-electrons redox reaction. Reproduced with permission from ref.97. Copyright 2018 American Chemical Society. BHT ligands: (h) Scheme of chemical structure of monolayer Ni-BHT complex (Gray-C, yellow- S, green-Ni). Reproduced with permission from ref.164. Copyright 2013 American Chemical Society.

Polyoxometalate (POM) is a class of metal-oxide-cluster anions, with the general units of MO<sub>x</sub> (M = V, Mo, W), which can perform multi-electron redox reactions and maintain structural stability during the electrochemical process. However, their high solubility in organic solvents limits their application in organic electrolyte battery systems because of the inevitable dissolutions of active materials and capacity fading. To decrease their solubility, POM-based MOFs, namely POMOFs, have been constructed through chelating metal centers and hetero-atoms in POM as well as other conventional ligands. As a result, POMOFs combine the advantages of multi-electron transfer of POMs and high structure stability of MOFs. Polymolybdates have been favourably chosen to synthesize POMOFs and demonstrated a promising electrochemical performance as reported by La and coauthors.<sup>148-151</sup> To prepare [PMo<sub>8</sub>VMo<sub>4</sub>O<sub>37</sub>(OH)<sub>3</sub>Zn<sub>4</sub>] [TPT]<sub>5</sub>\*2TPT\*2H<sub>2</sub>O (where TPT = tris-(4-pyridyl)triazine), namely NNU-11, the layers of Zn-ε-Keggin units linked by TPT ligands stack together to form a π - π stacking 3D array, where each Zn (II) ion coordinates with three bridging oxygen atoms from ε-Keggin fragment, while at the same time, four embedded Zn (II) ions chelate with two nitrogen atoms of two TPT ligands (Fig. 4a-b).<sup>149</sup> A stable capacity of 750 mAh g<sup>-1</sup> at 50 mA g<sup>-1</sup> within 0.01-3.0V (Vs. Li/Li<sup>+</sup>) is obtained over 200 cycles, which comes from (1) the reversible Zn<sup>2+</sup>/Zn and Mo<sup>6+</sup>/Mo<sup>4+</sup> redox couples and (2) the lithium

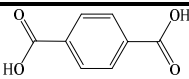
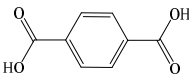
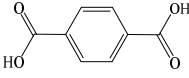
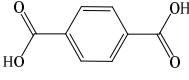
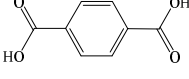
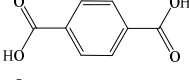
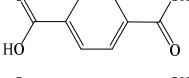
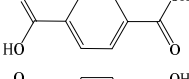
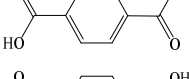
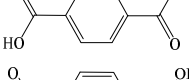
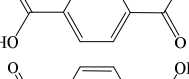
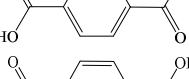
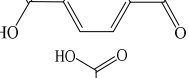
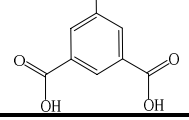
insertion/extraction movement at the uncoordinated N of pyridine. Interestingly, the existed π-π stacking factor provides the benefits that (1) improves the electronic conductivity and decreases the ohmic loss, and (2) provides more Li<sup>+</sup> storage sites by pseudo-capacitance behavior. Two thermally-stable POMOFs, NENU-506 (TBA)<sub>3</sub>[PMo<sub>8</sub>Mo<sup>VI</sup><sub>4</sub>O<sub>38</sub>(OH)<sub>2</sub>Zn<sub>4</sub>(IN)<sub>2</sub>] and NENU-507 (TBA)<sub>3</sub>[PMo<sup>V</sup><sub>8</sub>Mo<sup>VI</sup><sub>4</sub>O<sub>38</sub>(OH)<sub>2</sub>Zn<sub>4</sub>(PBA)<sub>2</sub>].H<sub>2</sub>O, (where IN = isonicotinic acid, TBA<sup>+</sup> = tetrabutylammonium ion, and HPBA = 4-(pyridin-4-yl) benzoic acid), are synthesized and employed in LIB anodes (0.01-3.0V, Vs. Li/Li<sup>+</sup>).<sup>151</sup> A better cycling performance is shown at NENU-507 electrode, which presents 640 mAh g<sup>-1</sup> over 100 cycles and ~ 96.68% capacity of the 2<sup>nd</sup> cycle. Material characterization reveals the redox active transitional metal ions (Mo and Zn), and Li<sup>+</sup> coordination interaction with organic ligands are devoted to the whole battery performance. Besides above-mentioned polymolybdate-POMOFs, the polyoxometalate units as building units for POMOF-based electrode materials also can be seen in [H<sub>3</sub>SiMo<sub>12</sub>O<sub>40</sub>], [H<sub>5</sub>SiMo<sub>12</sub>O<sub>40</sub>], [H<sub>5</sub>GeMo<sub>12</sub>O<sub>40</sub>], [H<sub>5</sub>PMo<sub>10</sub>V<sub>2</sub>O<sub>40</sub>], [H<sub>4</sub>PW<sub>12</sub>O<sub>40</sub>], [PW<sub>9</sub>O<sub>34</sub>], [V<sub>4</sub>O<sub>12</sub>] and so on.<sup>148, 150, 152-153</sup>

Motivated by the doping strategy that has been widespread in ameliorating conventional Li-rich layered oxides (Ni, Co, Mn) and Ti-based anode materials, bimetallic MOPs are investigated to ameliorate the coordination conditions and present better electrochemical performance than monometallic system.<sup>154-158</sup> One possible way to generate isostructural bimetallic MOPs is to utilize two metal ions with comparable ionic radii such as Zn (II, 0.74 Å) and Co (II, 0.72 Å). Isostructural CoZn-ZIF is prepared by 64% Co<sup>2+</sup> substitution of Zn<sup>2+</sup> in Zn-ZIF-8 crystal.<sup>159</sup> Hu et al. reported that only one Li<sup>+</sup> per unit can be intercalated into the imidazole rings of pristine ZIF, however, theoretically, over four Li<sup>+</sup> per unit could be inserted into CoZn-ZIF due to four N atoms per units participating in lithium ion storage. Interestingly, when CoZn-ZIF anodes are processed in the charge/discharge process, the Co-N bonds reversibly break/regenerate, while Zn-N bonds remain the same as in the redox process of Zn-ZIF-8. Upon setting the current density at 100 mA g<sup>-1</sup> and potential windows within 0.01 to 3.0 V (Vs. Li/Li<sup>+</sup>), CoZn-ZIF delivers a stable capacity of 605.8 mAh g<sup>-1</sup> over 100 cycles, while Zn-ZIF-8 and Co-ZIF-67 only exhibit the capacities of 94.8 mAh g<sup>-1</sup> and 122 mAh g<sup>-1</sup>, respectively. Another method is to introduce a certain amount of larger metal ions to broaden the interlayer distance and support a stable structure. In this way, enough space for ion diffusion and a reduction of charge-transfer resistance are ensured.<sup>160-161</sup> A simple microwave-assisted method, where HCl is utilized to adjust the morphology of MOFs, is applied to synthesize Zn doped Ni-MOF. During the synthesis process, crystal growth and agglomeration are controlled by the amount of doped Zn ions and modulator HCl. As a result, a honeycomb-like hierarchical spherical Zn-doped Ni-MOFs is obtained and the interlayers are enlarged by ~0.09 nm. When the ratio is Zn/Ni=0.07, the high capacities of 237.4 mAh g<sup>-1</sup> (1 A g<sup>-1</sup>) and 122.3 mAh g<sup>-1</sup> (20 A g<sup>-1</sup>) are obtained, respectively. A similar approach has been adopted to prepare Co-doped Mn-BTC and Zn-doped Fe-BDC@300, which exhibit high capacity of 901 mAh g<sup>-1</sup> after 150 cycles and 863.4 mAh g<sup>-1</sup> over 120 cycles, respectively, within 0.01-3.0 V (Vs. Li/Li<sup>+</sup>) at 100 mA g<sup>-1</sup> (Fig. 4c-d shows the example of Fe(Zn)-BDC@300).<sup>126, 161</sup>

## Journal Name

## ARTICLE

**Table 1** A list of organic ligands and corresponding electrochemical performance of MOPs (NM=Do not mention)

Ligand name	Ligand structure	Molecular name formula	Morphology	Capacity (mAh g <sup>-1</sup> ) Current density Cycling times	Potential (V)	Ref.
1,4-benzenedicarboxylate (H <sub>2</sub> BDC)		MIL-53(Fe) [Fe <sup>III</sup> (OH) <sub>0.8</sub> F <sub>0.2</sub> (O <sub>2</sub> CC <sub>6</sub> H=CO <sub>2</sub> ) <sub>2</sub> ]	NM	70, 10.7 mA g <sup>-1</sup> , 50 <sup>th</sup>	1.5~3.5, Vs. Li/Li <sup>+</sup>	98
1,4-benzenedicarboxylate (H <sub>2</sub> BDC)		MIL-68(Fe) Fe(OH)(BDC)·(DMF) <sub>x</sub> x ≈ 1.1	NM	40, C/50 0.35Li per Fe, 12 <sup>th</sup>	1.5~3.5, Vs. Li/Li <sup>+</sup>	165
1,4-benzenedicarboxylate (H <sub>2</sub> BDC)		MIL-101(Fe)	NM	0.37 Li/Fe (1 Li/Fe=107.74), C/40, 5 <sup>th</sup>	2.0~3.5, Vs. Li/Li <sup>+</sup>	166
1,4-benzenedicarboxylate (H <sub>2</sub> BDC)		Fe-MIL-88B [Fe <sub>3</sub> O(BDC) <sub>3</sub> (H <sub>2</sub> O) <sub>2</sub> (NO <sub>3</sub> ) <sub>3</sub> ] <sub>n</sub>	Polyhedral Nanorods	744.5, 100 mA g <sup>-1</sup> , 400 <sup>th</sup>	0.005~3.0, Vs. Li/Li <sup>+</sup>	167
1,4-benzenedicarboxylate (H <sub>2</sub> BDC)		Co-MOFs Co <sub>2</sub> (OH) <sub>2</sub> BDC	NM	650, 50 mA g <sup>-1</sup> , 100 <sup>th</sup>	0.02~3.0, Vs. Li/Li <sup>+</sup>	115
1,4-benzenedicarboxylate (H <sub>2</sub> BDC)		Co-MOFs Co(1,4-BDC)(DMF) <sub>0.61</sub>	Shale-shaped	1090, 200 mA g <sup>-1</sup> , 100 <sup>th</sup>	0.01~3.0, Vs. Li/Li <sup>+</sup>	114
1,4-benzenedicarboxylate (H <sub>2</sub> BDC)		Co-MOFs Co <sub>2</sub> (OH) <sub>2</sub> BDC	Microflowers	1345, 100 mA g <sup>-1</sup> , 100 <sup>th</sup>	0.01~3.0, Vs. Li/Li <sup>+</sup>	113
1,4-benzenedicarboxylate (H <sub>2</sub> BDC)		Co-MOFs Co <sub>2</sub> (OH) <sub>2</sub> tp	Nanosheets	555, 50 mA g <sup>-1</sup> , 50 <sup>th</sup>	0.01~3.0, Vs. Na/Na <sup>+</sup>	124
1,4-benzenedicarboxylate (H <sub>2</sub> BDC)		Co-MOFs L-Co <sub>2</sub> (OH) <sub>2</sub> BDC	Layers	188, 1000mA g <sup>-1</sup> , 600 <sup>th</sup>	0.2~3.0, Vs. K/K <sup>+</sup>	168
1,4-benzenedicarboxylate (H <sub>2</sub> BDC)		Cu-BDC MOFs [Cu <sub>2</sub> (C <sub>8</sub> H <sub>4</sub> O <sub>4</sub> ) <sub>4</sub> ] <sub>n</sub>	Particles	161, 48 mA g <sup>-1</sup> , 50 <sup>th</sup>	0.01~2.5, Vs. Li/Li <sup>+</sup>	89
1,4-benzenedicarboxylate (H <sub>2</sub> BDC)		Mn-BDC MOFs Mn <sub>3</sub> (BDC) <sub>3</sub> (μDMF) <sub>2</sub>	Loose Homogeneous Laminar	974, 100 mA g <sup>-1</sup> , 100 <sup>th</sup>	0.01~3.0, Vs. Li/Li <sup>+</sup>	135
1,4-benzenedicarboxylate (H <sub>2</sub> BDC)		MIL-47 (V) V <sup>IV</sup> (O)(bdc)	NM	82, 10 mA g <sup>-1</sup> , 50 <sup>th</sup>	1.5~4.0, Vs. Li/Li <sup>+</sup>	105
1,4-benzenedicarboxylate (H <sub>2</sub> BDC)		UiO-66 (Zr) Zr <sub>6</sub> O <sub>4</sub> (OH) <sub>4</sub> (BDC) <sub>6</sub>	Nanoparticles	118, 80 mA g <sup>-1</sup> , 30 <sup>th</sup>	0.01~3.0, Vs. Li/Li <sup>+</sup>	169
1,3,5- benzenetricarboxylate (BTC)		MIL-100(Fe) Fe <sup>III</sup> <sub>3</sub> O(H <sub>2</sub> O) <sub>2</sub> F[C <sub>6</sub> H <sub>3</sub> (CO <sub>2</sub> ) <sub>3</sub> ] <sub>2</sub> ·nH <sub>2</sub> O	Mesoporous Cages,	10, 9.3 mA g <sup>-1</sup> , 30 <sup>th</sup>	1.5~4.0, Vs. Na/Na <sup>+</sup>	170

Ligand name	Ligand structure	Molecular name formula	Morphology	Capacity (mAh g <sup>-1</sup> ) Current density Cycling times	Potential (V)	Ref.
1,3,5-benzenetricarboxylate (BTC)		MIL-100(Fe) $\text{Fe}^{\text{III}}_3\text{O}(\text{H}_2\text{O})_2\text{F}[\text{C}_6\text{H}_3(\text{CO}_2)_3]_2 \cdot 2\text{H}_2\text{O}$	Nanoparticles	10, 31 mA g <sup>-1</sup> , 30 <sup>th</sup>	0~1.0, Vs. Na/Na <sup>+</sup>	103
1,3,5-benzenetricarboxylate (BTC)		F300-like Fe-BTC	Basolite F300-like	1021, 100 mA g <sup>-1</sup> , 100 <sup>th</sup>	0.001~3.0, Vs. Li/Li <sup>+</sup>	126
1,3,5-benzenetricarboxylate (BTC)		Ni-BTC <sub>EtOH</sub> MOF	Flower-like	1100, 200 mA g <sup>-1</sup> , 100 <sup>th</sup>	0.01~3.0, Vs. Li/Li <sup>+</sup>	109
1,3,5-benzenetricarboxylate (BTC)		CoBTC-EtOH CPs	Hollow Microspherical	473, 2000 mA g <sup>-1</sup> , 500 <sup>th</sup>	0.01~3.0, Vs. Li/Li <sup>+</sup>	171
1,3,5-benzenetricarboxylate (BTC)		Cu-MOFs Cu <sub>3</sub> (BTC) <sub>2</sub>	Octahedral Shaped	740, 96 mA g <sup>-1</sup> , 50 <sup>th</sup>	0.01~3.0, Vs. Li/Li <sup>+</sup>	111
1,3,5-benzenetricarboxylate (BTC)		Mn-MOFs Mn <sub>3</sub> (BTC) <sub>2</sub>	Porous Sheets	694, 100 mA g <sup>-1</sup> , 100 <sup>th</sup>	0.01~2.0, Vs. Li/Li <sup>+</sup>	112
1,3,5-benzenetricarboxylate (BTC)		MOF-177 (Zn) Zn <sub>4</sub> O(BTC) <sub>2</sub>	Microcubes	105, 50 mA g <sup>-1</sup> , 50 <sup>th</sup>	0.05~1.6, Vs. Li/Li <sup>+</sup>	85
1,2,4,5-benzenetetracarboxylic acid (H <sub>4</sub> BTCA)		Co-BTCA CPs	Lamellar	801.3, 200 mA g <sup>-1</sup> , 50 <sup>th</sup>	0.01~3.0, Vs. Li/Li <sup>+</sup>	96
1,4-naphthalenedicarboxylate (NDC)		Zn-NDC CPs	Big Brick-like Particles	468.9, 100 mA g <sup>-1</sup> , 100 <sup>th</sup>	0.05~3.0, Vs. Li/Li <sup>+</sup>	172
1,4-naphthalenedicarboxylate (NDC)		Mn-MOFs Mn <sub>2</sub> (NDC) <sub>2</sub> (DMF) <sub>2</sub>	Bar	765.4, 200 mA g <sup>-1</sup> , 300 <sup>th</sup>	0.01~3.0, Vs. Li/Li <sup>+</sup>	118
2,6-naphthalene dicarboxylate (Naph)		iMOF 2,6-Naph(COOLi) <sub>2</sub>	layers	220	0.7, Vs. Li/Li <sup>+</sup>	173
4,4'-dioxidobiphenyl-3,3'-dicarboxylate (Dobpdc)		Fe <sub>2</sub> (dobpdc) MOFs	3D Framework with Pores	90, 1C, 50 <sup>th</sup>	2.0~3.65, Vs. Na/Na <sup>+</sup>	174

Journal Name			ARTICLE			
Ligand name	Ligand structure	Molecular name formula	Morphology	Capacity (mAh g <sup>-1</sup> ) Current density Cycling times	Potential (V)	Ref.
2,5-dioxido-1,4-benzenedicarboxylate (DOBDC)		Co <sub>2</sub> (DOBDC) MOFs	Rod-like Prism	526.1, 500 mA g <sup>-1</sup> , 200 <sup>th</sup>	0.01~3.0, Vs. Li/Li <sup>+</sup>	117
2,5-furandicarboxylate		CoC <sub>6</sub> H <sub>2</sub> O <sub>5</sub> (H <sub>2</sub> O) <sub>2</sub> CPs	Hollow Microspheres	549.8, 100 mA g <sup>-1</sup> , 95 <sup>th</sup>	0.05~3.0, Vs. Li/Li <sup>+</sup>	175
Formic acid		Zn <sub>3</sub> (HCOO) <sub>6</sub> MOFs	Diamondoid	560, 60 mA g <sup>-1</sup> , 60 <sup>th</sup>	0.005~3.0, Vs. Li/Li <sup>+</sup>	86
Formic acid		[Ni <sub>3</sub> (HCOO) <sub>6</sub> ] MOFs/CNTs	Microsized Ellipsoidal Particles	560, 300 mA g <sup>-1</sup> , 400 <sup>th</sup>	0.01~3.0, Vs. Li/Li <sup>+</sup>	176
Aspartic acid (Asp)		Cu-Asp CPS	Nanofibers	233, 50 mA g <sup>-1</sup> , 200 <sup>th</sup>	0.01~3.0, Vs. Li/Li <sup>+</sup>	177
Fumaric acid		Al-FumAs MOFs	Tremella-like	392, 37.5 mA g <sup>-1</sup> , 100 <sup>th</sup>	0.01~3.0, Vs. Li/Li <sup>+</sup>	140
2,7-anthraquinonedicarboxylic acid (2,7-H <sub>2</sub> AQDC)		[Cu(2,7-AQDC)(DMF)] <sub>∞</sub> ·xDMF (1·DMF) MOFs	Microporous	105, 1mA, 50 <sup>th</sup>	1.7~4.0, Vs. Li/Li <sup>+</sup>	129
2,7-anthraquinonedicarboxylic acid (2,7-H <sub>2</sub> AQDC)		Mn <sub>7</sub> (2,7-AQDC) <sub>6</sub> (2,6-AQDC) <sub>6</sub> (DMA) <sub>6</sub> MOFs	NM	190, 1mA, 50 <sup>th</sup>	1.0~4.5, Vs. Li/Li <sup>+</sup>	133
Croconic acid		[M(C <sub>5</sub> O <sub>5</sub> )(H <sub>2</sub> O) <sub>3</sub> ] <sub>n</sub> (M = Mn and Co) CPs	NM	729, 100 mA g <sup>-1</sup> , 140 <sup>th</sup>	0.01~2.4, Vs. Li/Li <sup>+</sup>	178
Tetrahydroxybenzoquinone (THBQ)		P(THBQ-Al) CPs	NM	113, 100 mA g <sup>-1</sup> , 100 <sup>th</sup>	1.5~3.0, Vs. Na/Na <sup>+</sup>	179
2,5-dihydroxy-1,4-benzoquinone (2,5-DBQ)		[Li <sub>2</sub> (C <sub>6</sub> H <sub>2</sub> O <sub>4</sub> )] CPs	NM	137, 100 mA g <sup>-1</sup> , 100 <sup>th</sup>	1.5~3.5, Vs. Li/Li <sup>+</sup>	142
Hexaaminobenzene (HAB)		NiDI 2D MOFs Ni(L <sup>isq</sup> ) <sub>2</sub> L <sup>isq</sup> =HAB	2D Coordination Networks	155, 250 mA g <sup>-1</sup> , 300 <sup>th</sup>	3.0~4.5, Vs. Li/Li <sup>+</sup>	132

Ligand name	Ligand structure	Molecular name formula	Morphology	Capacity (mAh g <sup>-1</sup> ) Current density Cycling times	Potential (V)	Ref.
Hexaaminobenzene (HAB)		Co-HAB 2D MOFs	NM	226, 500 mA g <sup>-1</sup> , 50 <sup>th</sup>	0.05~2.5, Vs. Na/Na <sup>+</sup>	97
Imidazole (IM) 2-aminobenzimidazole (abIM)		Zn(IM) <sub>1.5</sub> (abIM) <sub>0.5</sub> MOFs	Porous	190, 100 mA g <sup>-1</sup> , 200 <sup>th</sup>	0.01~3.0, Vs. Li/Li <sup>+</sup>	122.
2-methylimidazole (Hmim)		ZIF-8 Zn(Hmim) <sub>2</sub>	Nanoparticles	335.3, 23.4 mA g <sup>-1</sup> , 100 <sup>th</sup>	0.01~3.0, Vs. Li/Li <sup>+</sup>	123
2-methylimidazole (Hmim)		ZIF-67 Co(Hmim) <sub>2</sub>	Nanoparticles	311.6, 24 mA g <sup>-1</sup> , 100 <sup>th</sup>	0.01~3.0, Vs. Li/Li <sup>+</sup>	123
7,7,8,8- tetracyanoquinodimetha ne (TCNQ)		Cu <sup>I</sup> TCNQ	NM	214, 50 mA g <sup>-1</sup> , 50 <sup>th</sup>	2.0~4.1, Vs. Li/Li <sup>+</sup>	180
Terephthalonitrile (BDCN)		Co-BDCN CPs	Nanowire	1132, 100 mA g <sup>-1</sup> , 100 <sup>th</sup>	0.01~3.0, Vs. Li/Li <sup>+</sup>	121
Tricarboxytriphenyl amine (H <sub>3</sub> TCA)		Cu-TCA MOFs	Porous	45, 2C, 200 <sup>th</sup> 1C=145 mAh g <sup>-1</sup>	1.4~4.3, Vs. Li/Li <sup>+</sup>	128
Tetrakis (4- carboxyphenyl)porphyrin (TCPP)		PCN-600 (Fe) MOFs	Needle-like	610, 400 mA g <sup>-1</sup> , 760 <sup>th</sup>	0.01~3.0, Vs. Li/Li <sup>+</sup>	181
3,3',5,5'-tetramethyl-4,4'- bipyrazole (H <sub>2</sub> Me4bpz)		Ni-Me4bpz MOFs	Wavy Layered	200, 50 mA g <sup>-1</sup> , 100 <sup>th</sup>	0.01~3.0, Vs. Li/Li <sup>+</sup>	90
Adenine (ade)		[Co <sub>2</sub> {ade} <sub>2</sub> (V <sub>4</sub> O <sub>12</sub> )(H <sub>2</sub> O) <sub>2</sub> ] CPs	NM	410, 50 mA g <sup>-1</sup> , 80 <sup>th</sup>	0.01~3.0, Vs. Li/Li <sup>+</sup>	152
Adenine (ade)		[Cd <sub>2</sub> {ade} <sub>2</sub> (V <sub>4</sub> O <sub>12</sub> )(H <sub>2</sub> O) <sub>2</sub> ] CPs	NM	485, 50 mA g <sup>-1</sup> , 80 <sup>th</sup>	0.01~3.0, Vs. Li/Li <sup>+</sup>	152
Benzenehexathiol (BHT)		Cu-BHT [Cu <sub>3</sub> (C <sub>6</sub> S <sub>6</sub> )] <sub>n</sub>	Thin Films	NM	NM	182
5-hydroxynicotinic acid (H <sub>2</sub> NA)		[Co(NA)] <sub>n</sub> CPs	NM	455, 100 mA g <sup>-1</sup> , 60 <sup>th</sup>	0.01~3.0, Vs. Li/Li <sup>+</sup>	94

Journal Name				ARTICLE		
Ligand name	Ligand structure	Molecular name formula	Morphology	Capacity (mAh g <sup>-1</sup> ) Current density Cycling times	Potential (V)	Ref.
5-hydroxynicotinic acid (H <sub>2</sub> NA)		[Ni(NA)] <sub>n</sub> CPs	NM	618, 100 mA g <sup>-1</sup> , 100 <sup>th</sup>	0.01~3.0, Vs. Li/Li <sup>+</sup>	94
4,5-imidazoledicarboxylic acid (idca)		CoH <sub>2</sub> IMDC·H <sub>2</sub> O CPs (H <sub>2</sub> IMDC=idca)	Microsphere- like	416.1, 1A g <sup>-1</sup> , 143 <sup>th</sup>	0.05~3.0, Vs. Li/Li <sup>+</sup>	183
4,5-imidazoledicarboxylic acid (idca)		LiZn CPs Li <sub>5</sub> Zn <sub>6</sub> C <sub>25</sub> H <sub>11</sub> N <sub>10</sub> O <sub>24</sub>	Elongated Polyhedron	133, 50 mA g <sup>-1</sup> , 100 <sup>th</sup>	0.01~3.0, Vs. Li/Li <sup>+</sup>	158
5-aminoisophthalic acid		Co(L) MOF Co(L)(H <sub>2</sub> O)] <sub>n</sub> ·2nH <sub>2</sub> O	NM	206, 500 mA g <sup>-1</sup> , 330 <sup>th</sup>	0.01~3.0, Vs. Na/Na <sup>+</sup>	134
5-aminoisophthalic acid		Cd(L) MOF Cd(L)(H <sub>2</sub> O)] <sub>n</sub> ·2nH <sub>2</sub> O	NM	166, 500 mA g <sup>-1</sup> , 330 <sup>th</sup>	0.01~3.0, Vs. Na/Na <sup>+</sup>	134
2,6-pyridinedicarboxylic acid		Zn 2,6-pyridinedicarboxylate CPs ZnC <sub>7</sub> H <sub>3</sub> NO <sub>4</sub>	Micro-Platelet- like	513.4, 100 mA g <sup>-1</sup> , 80 <sup>th</sup>	0.01~3.0, Vs. Li/Li <sup>+</sup>	184
3, 5-pyridinedicarboxylic acid (3, 5-H <sub>2</sub> PDC)		[Mn (3, 5-PDC)•3H <sub>2</sub> O] CPs	Irregular Particles	554, 100 mA g <sup>-1</sup> , 240 <sup>th</sup>	0.05~3.0, Vs. Li/Li <sup>+</sup>	185
4-hydroxypyridine-2,6- dicarboxylic acid		[Co <sub>1.5</sub> L(H <sub>2</sub> O) <sub>4</sub> ] <sub>n</sub> CPs	NM	431, 50 mA g <sup>-1</sup> , 50 <sup>th</sup>	0.01~3.0, Vs. Li/Li <sup>+</sup>	186
Nitrilotriacetic acid (HNta)		CoHNta CPs Co <sub>3</sub> [N (CH <sub>2</sub> COO) <sub>3</sub> ] <sub>2</sub>	Nanorods	875, 100 mA g <sup>-1</sup> , 300 <sup>th</sup>	0.01~3.0, Vs. Li/Li <sup>+</sup>	187
4,4'-bipyridine (4,4'-bpy) Tetrafluoroterephthalic acid (H <sub>2</sub> tfbdc)		Zn-LMOF [Zn(4,4'-bpy) (tfbdc)(H <sub>2</sub> O) <sub>2</sub> ]	Nanosheets	623, 50 mA g <sup>-1</sup> , 100 <sup>th</sup>	0.01~3.0, Vs. Li/Li <sup>+</sup>	91

Ligand name	Ligand structure	Molecular name formula	Morphology	Capacity (mAh g <sup>-1</sup> ) Current density Cycling times	Potential (V)	Ref.
4,4'-bipyridine (4,4'-bpy) Tetrafluoroterephthalic acid (H <sub>2</sub> tfbdc)		Ni-MOF [Ni(4,4'-bpy) (tfbdc)(H <sub>2</sub> O) <sub>2</sub> ]	Nanoparticles	406, 50 mA g <sup>-1</sup> , 50 <sup>th</sup>	0.01~3.0, Vs. Li/Li <sup>+</sup>	136
4,4'-bipyridine (4,4'-bpy) Tetrafluoroterephthalic acid (H <sub>2</sub> tfbdc)		Mn-LCP CPs [Mn-(tfbdc) (4,4'-bpy)(H <sub>2</sub> O) <sub>2</sub> ]	Layered	390, 50 mA g <sup>-1</sup> , 50 <sup>th</sup>	0.01~2.5, Vs. Li/Li <sup>+</sup>	88
4,4'-bipyridine (4,4'-bpy) Tetrafluoroterephthalic acid (H <sub>2</sub> tfbdc)		Co-LCP [Co(tfbdc)(4,4'-bpy)(H <sub>2</sub> O) <sub>2</sub> ]	Nanosheets	545, 50 mA g <sup>-1</sup> , 50 <sup>th</sup>	0.1~3.0, Vs. Li/Li <sup>+</sup>	92
Tetrafluoroterephthalic acid (H <sub>2</sub> tfbdc)		Co-TFBDC CPs	Nanosphere	1074.6, 100 mA g <sup>-1</sup> , 50 <sup>th</sup>	0.01~3.0, Vs. Li/Li <sup>+</sup>	188
3-methyl-1H-pyrazole-4- carboxylic acid (H <sub>2</sub> mpca) Tetrafluoroterephthalic acid (H <sub>2</sub> tfbdc)		Zn-ODCP CPs [Zn-(H <sub>2</sub> mpca) <sub>2</sub> (tfbdc)(H <sub>2</sub> O)]	Nanorods	300, 50 mA g <sup>-1</sup> , 50 <sup>th</sup>	0.1~3.0, Vs. Li/Li <sup>+</sup>	87
3-methyl-1H-pyrazole-4- carboxylic acid (H <sub>2</sub> mpca) Tetrafluoroterephthalic acid (H <sub>2</sub> tfbdc)		Cu-CPs [Cu(H <sub>2</sub> mpca)(tfbdc)]	Nanoparticles	375 F g <sup>-1</sup> , 2 A g <sup>-1</sup> , 1500 <sup>th</sup>	0~0.6, Vs. Li/Li <sup>+</sup>	189
4-(4-carboxyphenyl) pyridine N-oxide (4,4'- ocppy)		Pb-MOF [Pb(4,4'-ocppy) <sub>2</sub> ·7H <sub>2</sub> O]	NM	489, 100 mA g <sup>-1</sup> , 500 <sup>th</sup>	0.01~3.0, Vs. Li/Li <sup>+</sup>	137
1,1'-bis(3,5- dicarboxylatophenyl)- 4,4'-bipyridinium (bpybdc) Azide		[Co(H <sub>2</sub> O) <sub>6</sub> ][Co <sub>6</sub> (bpybdc) <sub>2</sub> (N <sub>3</sub> ) <sub>10</sub> (H <sub>2</sub> O) <sub>4</sub> ]·8H <sub>2</sub> O CPs	NM	510.4, 100 mA g <sup>-1</sup> , 200 <sup>th</sup>	0.01~3.0, Vs. Li/Li <sup>+</sup>	190
4-(4-pyridyl)benzoic acid N-oxide (4,4'-Hopybz) 4-(3-pyridyl)benzoic acid N-oxide (4,3'-Hopybz)		{[Pb(4,4'-opybz)(4,3'- opybz)]·3DMF·7H <sub>2</sub> O} <sub>n</sub> CPs	NM	405, 100 mA g <sup>-1</sup> , 100 <sup>th</sup>	0~3.0, Vs. Li/Li <sup>+</sup>	139
2,5-thiophenedicarboxylic acid (TDC)		Mn <sub>2</sub> (C <sub>6</sub> H <sub>2</sub> O <sub>4</sub> S)·2H <sub>2</sub> O	Microspheres	645.7, 400 mA g <sup>-1</sup> , 250 <sup>th</sup>	0.05~3.0, Vs. Li/Li <sup>+</sup>	191

Journal Name		ARTICLE				
Ligand name	Ligand structure	Molecular name formula	Morphology	Capacity (mAh g <sup>-1</sup> ) Current density Cycling times	Potential (V)	Ref.
2,5-thiophenedicarboxylic acid (TDC)		Co(TDC)(H <sub>2</sub> O) <sub>0.75</sub> CPs	Flower-like	328, 50 mA g <sup>-1</sup> , 100 <sup>th</sup>	0.01~3.0, Vs. Li/Li <sup>+</sup>	192
2,5-thiophenedicarboxylic acid (TDC)		CoTDC*1.5 H <sub>2</sub> O CPs	NM	1100, 100 mA g <sup>-1</sup> , 100 <sup>th</sup>	0.01~3.0, Vs. Li/Li <sup>+</sup>	193
2,5-thiophenedicarboxylic acid (TDC)		u-CoTDA MOFs	Randomly Arranged Flaky	790, 1000 mA g <sup>-1</sup> , 400 <sup>th</sup>	0.01~3.0, Vs. Li/Li <sup>+</sup>	125
Tetrathiafulvalenetetra- carboxylic Acid (TTF-TC)H <sub>4</sub>		MIL-132(K) K <sub>2</sub> (TTF-TC)H <sub>2</sub>	NM	~50, 10C 1C=59 mAh g <sup>-1</sup>	2.0~4.0, Vs. Li/Li <sup>+</sup>	143
Tetrathiafulvalenetetra- carboxylic Acid (TTF-TC)H <sub>4</sub>		MIL-136(Ni, Co) [[M(H <sub>2</sub> O) <sub>4</sub> ] <sub>2</sub> (TTF-TC)] <sub>3</sub> ·4H <sub>2</sub> O	NM	~ 20, 10 C	2.0-4.3, Vs. Li/Li <sup>+</sup>	131
N,N'-di(4-pyridyl)-1,4,5,8- naphthalenediimide (DPNDI)		[[Cd(NO <sub>3</sub> ) <sub>2</sub> (DPNDI)](DMA) <sub>2</sub> (H <sub>2</sub> O) <sub>0.5</sub> ] <sub>n</sub> MOFs	NM	~47, 100 mA g <sup>-1</sup> , 50 <sup>th</sup>	1.8-3.4, Vs. Li/Li <sup>+</sup>	194
N,N'-di(4-pyridyl)-1,4,5,8- naphthalenediimide (DPNDI)		[[Cd(ClO <sub>4</sub> ) <sub>2</sub> (DPNDI) <sub>2</sub> ] (DMA) <sub>4.5</sub> (H <sub>2</sub> O) <sub>2</sub> ] <sub>n</sub> MOFs	NM	~47, 100 mA g <sup>-1</sup> , 50 <sup>th</sup>	1.8-3.4, Vs. Li/Li <sup>+</sup>	194
5,5'-([4,4'-bipyridine]- 1,1'-diium-1,1'- diylbis(methylene)) Diisophthalate (L <sup>1</sup> ) Azide		[Co <sub>3</sub> (L <sup>1</sup> )(N <sub>3</sub> ) <sub>4</sub> ] MOFs	Pillared-Layer	618, 100 mA g <sup>-1</sup> , 200 <sup>th</sup>	0.01~3.0, Vs. Li/Li <sup>+</sup>	195
5,5'-([4,4'-bipyridine]- 1,1'-diium-1,1'- diylbis(methylene)) Diisophthalate (L <sup>1</sup> ) Azide		[Mn <sub>2</sub> (L <sup>1</sup> )(N <sub>3</sub> ) <sub>2</sub> (H <sub>2</sub> O) <sub>2</sub> ] <sub>3</sub> ·H <sub>2</sub> O MOFs	Pillared-Layer	358, 100 mA g <sup>-1</sup> , 200 <sup>th</sup>	0.01~3.0, Vs. Li/Li <sup>+</sup>	195
1,1'-bis(3,5- dicarboxylatophenyl)- 4,4'-bipyridinium (L <sup>2</sup> ) Azide		[Co <sub>4</sub> L <sup>2</sup> (N <sub>3</sub> ) <sub>6</sub> (H <sub>2</sub> O) <sub>2</sub> ] MOFs	Pillared-Layer	595, 100 mA g <sup>-1</sup> , 200 <sup>th</sup>	0.01~3.0, Vs. Li/Li <sup>+</sup>	195
1,1'-bis(3,5- dicarboxylatophenyl)- 4,4'-bipyridinium (L <sup>2</sup> ) Azide		[Mn <sub>4</sub> L <sup>2</sup> (N <sub>3</sub> ) <sub>6</sub> (H <sub>2</sub> O) <sub>2</sub> ] MOFs	Pillared-Layer	595, 100 mA g <sup>-1</sup> , 200 <sup>th</sup>	0.01~3.0, Vs. Li/Li <sup>+</sup>	195
Oxalic acid Phosphoric acid		Li <sub>2</sub> (VO) <sub>2</sub> (HPO <sub>4</sub> ) <sub>2</sub> (C <sub>2</sub> O <sub>4</sub> )	NM	47, 500 mA g <sup>-1</sup> , 20 <sup>th</sup>	2.5~4.5, Vs. Li/Li <sup>+</sup>	107
1,3,5- Benzenetriphosphonate (BTP)		Fe <sub>3</sub> (BTP)·3H <sub>2</sub> O MOFs	Particles	550, 80 mA g <sup>-1</sup> , 25 <sup>th</sup>	0.1~3.0, Vs. Li/Li <sup>+</sup>	196

### 3.2 Tuning and Functionalization of Bridging Ligands

It is believed that redox-active organic ligands play a more important role than metal nodes, concerning how to achieve prominent battery performance including good cyclability and high capacities. The metal-node-transfer redox electrons through the alternation between different oxidation states could lead to lower coordination stabilities with ligands, and the amount of exporting electrons is smaller due to the limited stable oxidation states of metal ions. However, organic ligands undergo lithium-ion insertion/extraction at the free functional groups, which have little influence on the whole coordination structure, ensuring an integrated structure even in high/low potential. Moreover, redox-active linkers can be able to provide various intercalation sites, resulting in higher specific capacity. Therefore, the discussion about optional bridging ligands among redox-active MOPs is essential.

Table 1 presents a list of MOPs-based electrode materials classified according to the types of organic ligands. The molecular information and battery performance are also included. In addition, the previously-reported functional carboxyl ligands are explained detailly in the last section. As for the synergistic effect from aromatic rings and N-functional groups at organic spacers, Chen et al. designed a new bi-functionalized MOF (BMOFs), composing of  $\text{Zn}(\text{IM})_{1.5}(\text{abIM})_{0.5}$ , which combs the hydrophobic and rigid merits of phenyl as well as the redox active N atoms of amine and imidazolate. The presence of the phenyl groups in the framework is able to increase the chemical and thermal stability. When treated in aqueous and organic solution at 60 °C for 15 days, BMOFs still present the same powder XRD peak as compared with original samples. Also, after exposing BMOFs at 200 °C in air for 3 days, it still retains an intact structure. Additionally, there is host-guest interactions between  $-\text{NH}_2$  or N atoms and  $\text{Li}^+$  ions, which helps BMOFs serving as anodes for LIBs. It exhibits about 190  $\text{mAh g}^{-1}$  at 100  $\text{mA g}^{-1}$  after 200 cycles and the value is equal to that of the 2<sup>nd</sup> cycle. Additionally, when cycled at 400  $\text{mAh g}^{-1}$ , the coulombic efficiency approaches 100% after 200 cycles.<sup>122</sup> Due to the vital progress of 2D electronic conductive MOFs analogues in battery study, the following paragraphs will focus on two meaningful ligands: (1) hexaaminobenzene (HAB) (Fig. 4g) and (2) benzenehexathiol (BHT) (Fig. 4h).

Starting from HAB ligands, electrically-conductive 2D-HAB-CPs have been studied in a great number of energy storage devices, ranging from experimental to computational investigations. As there is strong  $\pi-\pi$  interaction among the layers of M-HAB CPs ( $\text{M}=\text{Ni}^{\text{II}}$ ,  $\text{Cu}^{\text{II}}$  and  $\text{Co}^{\text{II}}$ ) nanosheets, a single layer cannot be obtained and samples are described as thick (about 1-2mm) or thin (lower than 10nm).<sup>197</sup> Porous 2D crystalline  $\text{Ni}_3(\text{HAB})_2$  and  $\text{Cu}_3(\text{HAB})_2$  MOFs are confirmed with excellent bulk electronic

conductivities over 800  $\text{S m}^{-1}$ , verifying a partially-occupied delocalized band of Fermi energy.<sup>198</sup> 2D  $\text{Co}^{\text{II}}$ -HAB MOFs achieved fast  $\text{Na}^+$  storage capability up to 214  $\text{mAh g}^{-1}$  at 2  $\text{A g}^{-1}$  within 0.5–3.0 V (Vs.  $\text{Na}/\text{Na}^+$ ), mainly because of its high bulk electrical conductivity (1.57  $\text{S cm}^{-1}$ ).<sup>97</sup> Thanks to ultra-small HAB linkers, after coordinating with  $\text{Cu}(\text{II})$  and  $\text{Ni}(\text{II})$ , a highly dense packed framework with outstanding volumetric capacitances ( $>760 \text{ F cm}^{-3}$ ) and gravimetric capacitance ( $>400 \text{ F g}^{-1}$ ) at 50  $\mu\text{m}$  electrode thickness is obtained.<sup>199</sup> Additionally, theoretical DFT calculation of 2D-HAB-CP can also be conducted to investigate its promising application in Li-S cathodes.<sup>200</sup>

According to the previous study,  $d^8$  transitional metal ions tend to form square-planar coordinating complexes and BHT ligands provide multi-chelating sites through a preferred equilateral-triangular direction. According to these theoretical results, a 2D-BHT-CPs  $\pi$ -stacking nanosheets is expected to be produced.<sup>164</sup> In 2004, Nishihara et al. found that Ni-bis(dithiolene) nanosheets with a conductivity of  $1.6 \times 10^2 \text{ S cm}^{-1}$  offered a foothold for further study.<sup>201</sup> Zhou et al. paid attention to 2D Cu-BHT CPs and applied it as Li-S battery cathodes and catalysts.<sup>67, 182, 202, 203</sup> They found that Cu-BHT CPs nanosheets, with the formula of  $[\text{Cu}_3(\text{C}_6\text{S}_6)]_n$ , present a high value conductivity of 1,580  $\text{S cm}^{-1}$  at RT, inducing from strong  $d-\pi$  conjugation and numerous delocalized electrons among 2D plane.<sup>182</sup> In addition, they also prepared novel 2D Ag-S networks, composing of  $[\text{Ag}_5(\text{C}_6\text{S}_6)]_n$  CPs layers, which demonstrate a high conductivity of  $\sim 250 \text{ S cm}^{-1}$  at 300 K.<sup>204</sup> In summary, future work could aim at  $\text{Li}^+/\text{Na}^+$  storage based on BHT ligands-CPs materials.<sup>205</sup> Since the bridging ligands have strong relationship to electrical conductivity and battery performance, preferential attention are required to focus on the selection and synthesis of suitable organic ligands.

### 3.3 Control and Enhancement of Electronic Conductivity

MOFs, prevailing over existing electrode materials (carbon-based,  $\text{Li}_x\text{M}_y\text{O}_z$   $x/y/z \geq 0$ , polyanion compounds and so on) with limited porous structure and chemical constituent,<sup>17, 206</sup> have been rapidly developed in energy storage and conversion devices due to the combination of rich ordered porosity and dispersed multi-redox active sites. The unique and abundant pores provide fast ion-diffusion channels and large contact areas between electrolytes and redox-reaction locus (metal nodes and bridging ligands). Therefore, theoretically,  $\sim 100\%$  utilization of whole MOFs could be obtained to accomplish superior energy/power density. However, even though a large number of electrons can be produced by the redox-reaction and ligand doping processes, the intrinsic insulation properties of MOFs trap some of these electrons and block them from transporting to the external circuit. There are two proposed

methods to solve this problem: (1) adding exterior conductive agents, including conducting carbon black, carbon nanotubes,<sup>108, 176</sup> functionalized graphene/reduced graphene oxide,<sup>127, 134, 148, 163, 207-209</sup> conductive polymers,<sup>210-212</sup> metal nanoparticles<sup>213</sup> and so on; and (2) enhancing interior conductivity via constructing electron and charge flowing routes based on each framework joints. The first way, which has been widely used in traditional and commercially-available  $\text{LiCoO}_2/\text{LiMn}_2\text{O}_4/\text{LiFePO}_4$  electrodes, could be applied to MOFs electrodes. Among those conductive species, chemically-modified CNTs and RGO, especially with carboxyl groups, could not only enhance the electron-conductive properties but also act as the precursors to build further frameworks and morphologies. The interconnected electron/ion transport pathways among  $\text{Co}_2(\text{OH})_2\text{BDC}$  MOF and  $\text{COOH}$ -graphene (named CoCGr) are realized by chelating the  $\text{-COOH}$  groups in  $\text{COOH}$ -graphene and  $\text{Co}^{2+}$  through an *in situ* solvothermal treatment, where the localized state of three free electrons in high-spin  $\text{Co}^{2+}$  nodes is converted to be delocalized state once  $\text{Li}^+$  ions impregnation (Fig. 4e-f).<sup>163</sup> CoCGr-5 (5 wt% of carboxyl graphene) presents a smaller semicircle in EIS test (less than 20  $\Omega$ ) than that of pristine  $\text{Co}_2(\text{OH})_2\text{BDC}$  (about 60  $\Omega$ ), demonstrating a reduced resistance among electrodes. The enhanced electron-conducting ability is helpful to achieve an improved rate capability. Pristine  $\text{Co}_2(\text{OH})_2\text{BDC}$  and CoCGr-5, when cycled between 0.01-3.0 V in LIBs, present  $\sim 1081 \text{ mAh g}^{-1}$  and  $\sim 1331 \text{ mAh g}^{-1}$  at 100  $\text{mA g}^{-1}$ ,  $\sim 937 \text{ mAh g}^{-1}$  and  $\sim 1307 \text{ mAh g}^{-1}$  at 200  $\text{mA g}^{-1}$ ,  $\sim 784 \text{ mAh g}^{-1}$  and  $\sim 1195 \text{ mAh g}^{-1}$  at 400  $\text{mA g}^{-1}$ ,  $\sim 644 \text{ mAh g}^{-1}$  and  $\sim 1089 \text{ mAh g}^{-1}$  at 600  $\text{mA g}^{-1}$ ,  $\sim 457 \text{ mAh g}^{-1}$  and  $\sim 919 \text{ mAh g}^{-1}$  at 1 A  $\text{g}^{-1}$ ,  $\sim 248 \text{ mAh g}^{-1}$  and  $\sim 555 \text{ mAh g}^{-1}$  at 2 A  $\text{g}^{-1}$ , respectively. Additionally, CoCGr-5 electrode declares long cycling life, by maintaining a capacity of 818  $\text{mAh g}^{-1}$  at 1 A  $\text{g}^{-1}$  after 400 cycles. Yang et al.<sup>207</sup> utilized terephthalic acid-GO to provide effective nucleation sites and structure-guiding template to grow Mn-MOF. The reversible discharge capacity of Mn-MOF/RGO stabilizes at  $\sim 432 \text{ mA h g}^{-1}$  (500  $\text{mA g}^{-1}$ ) and 348  $\text{mA h g}^{-1}$  (1000  $\text{mA g}^{-1}$ ) at 500 cycles (0.01-3 V vs.  $\text{Li/Li}^+$ ). Besides increasing electrical conductivity, the variation of material morphology could also be accompanied with the loading of carbon species. After decorating  $\text{Ni}(\text{TA})$  ( $\text{Ni}_2$ -trimesic acid) with  $\text{COOH}$ -MWCNT through a hydrothermal synthesis process, 2 to 5  $\mu\text{m}$  microspheric  $\text{Ni}(\text{TA})$  particles with low surface areas totally turn into flower-shaped-cluster sheets with the thickness of only  $\sim 13 \text{ nm}$ .<sup>108</sup> The specific capacity raises from 94  $\text{mAh g}^{-1}$   $\text{Ni}(\text{TA})$  to 115  $\text{mAh g}^{-1}$   $\text{MWCNTs@Ni}(\text{TA})$  at 2 A  $\text{g}^{-1}$ .

In conclusion, the anchored MOFs with functionalized CNTs/RGO show several advantages including: (1) enhanced electron-conductivity, therefore higher rate capability; (2) the avoidance of MOFs particles self-aggregation during the synthesis process; (3) the buffered volume expansion during lithiation/delithiation process; (4) the optimized material morphologies and pore structures via adjusting carbon species concentration; and (5) the improved mechanical flexibility due to the additives of soft carbon. However, the exterior conductive additives are inactive and account for volume and mass percentage of the electrode, which leads to a lower energy density ( $\text{MJ kg}^{-1}$ ,  $\text{MJ L}^{-1}$ ) of the whole electrode. Therefore, a

simple and stable way to counteract the low intrinsic electronic conductivity of MOFs should be taken to overcome the low level of effective lithiation/de-lithiation at high current density.

Many MOFs are intrinsically insulating due to their localized electrons in atoms or bonds that cannot flow along molecular orbits, letting alone to external circuit.<sup>214</sup> Several related reviews on conductive MOFs have summarized the general design principles, experiment strategies, and characterization techniques to help switching on their electron-conductivity.<sup>215-217</sup> The following will mainly focus on recent conductive MOFs that have been used as reversible electrode materials.

The important property of this category MOFs is that they display a good stability in severe chemical environments, such as over high/low potential and current, various organic/inorganic electrolyte solvents and solutes, repeatable lithiation/delithiation processes over many cycles and so on. In order to effectively utilize electronic conductivity of MOFs while maintaining their unique frameworks during the electrochemical reaction process, 2D conductive networks are realized by extending  $\text{p-}\pi/\text{d-}\pi$  conjugation in-plane for overlapping  $\pi$  orbits between organic ligands and metal nodes, and conducted through  $\pi$ - $\pi$  stacking interaction between layers.<sup>218</sup> Bao et al. firstly prepared 2D conductive Co-HAB MOFs (HAB= Hexaaminobenzene) for sodium ion storage, where three electrons and  $\text{Na}^+$  could be reversibly stored at each HAB ligand, showing 312  $\text{mAh g}^{-1}$  of theoretical capacity.<sup>97</sup> The extended  $\text{d-}\pi$  conjugation in 2D plane generates a bulk electric-conductivity of  $\sim 1.57 \text{ S cm}^{-1}$  as well as a high power ability of 214  $\text{mAh g}^{-1}$  (in 7 min) or 152  $\text{mAh g}^{-1}$  (in 45 s). What's more, the same HAB ligands have been used to fabricate Cu-HAB and Ni-HAB, exhibiting  $11 \pm 3 \text{ S m}^{-1}$  and  $70 \pm 15 \text{ S m}^{-1}$  at room temperature (RT) respectively, through the similar  $\text{d-}\pi$  conjugation theory.<sup>199</sup> Additionally, 2D MOFs constructed by  $\pi$ - $\pi$  stacking layered structure also play an important role in overcoming their insulating limitation.  $\text{Ni}_3(\text{HITP})_2$  (HITP = 2,3,6,7,10,11-hexaiminotriphenylene) is reported as the first neat MOFs electrode solely working for electrochemical double layer capacitors (EDLCs).<sup>219</sup> Delocalized electrons can flow through the  $\pi$ - $\pi$  conjugated electron cloud between 2D layers of  $\text{Ni}_3(\text{HITP})_2$  and over 5,000  $\text{S m}^{-1}$  of bulk electrical conductivity is presented.  $\text{Ni}_3(\text{HITP})_2$  electrodes exhibit the value of  $\sim 18 \mu\text{F cm}^{-2}$  for normalized specific surface area capacitance. It also shows a 90% capacitance retention in the range of 0-1V at 2A  $\text{g}^{-1}$  after  $10^4$  cycles. Similar 2D  $\pi$ - $\pi$  conjugated stacking sheets appear at electronic-conducting iMOF (2,6-Naph( $\text{COOLi}$ )<sub>2</sub>, 2,6-naphthalene dicarboxylate dilithium), specifically in repeating  $\pi$ -stacking naphthalene layers.<sup>220-221</sup> A full battery is assembled when iMOF is applied as a negative electrode and  $\text{LiNi}_{0.5}\text{Mn}_{1.5}\text{O}_4$  is a positive electrode in a laminate-type cell. The specific energy/power density can reach up to 300  $\text{Wh kg}^{-1}$  and 5  $\text{kW kg}^{-1}$ , respectively. Also, the capacity can retain 96% after 100 charge/discharge cycles. Ogihara et al. found that the crystal order of iMOF could be controlled and adjusted at post-annealing treatment, where the impurities generated in layers could be avoided during molecular self-assembly process. It is revealed that post-annealing at 623 K under Ar atmosphere is an effective way to reduce the length of the c-axis, which

reflects the distance of  $\pi$ - $\pi$  stacking naphthalene interlayers, so that iMOF electrodes show lower internal resistance and higher specific capacities.<sup>173</sup>

### 3.4 Realization of High Operation Voltage - Cathodes Applications

As the significant component in whole battery, cathodes mainly decide the working voltage range of batteries and thus the overall energy density. In order to satisfy the market demand for portable energy devices, some commercially-available cathode materials, such as  $\text{LiCoO}_2$  and  $\text{LiFePO}_4$ , have been developed. But their limited capacity ( $\sim 150 \text{ mAh g}^{-1}$ ) and variable structures in high operating potentials are the driving forces to search novel cathode materials for the enhancement of energy densities. MOFs, combining the merits of (1) co-redox active metal nodes and bridging ligands, (2) ordered and tunable pores and channels, and (3) robust framework during lithiation/delithiation process, become desirable cathodes with multi-electron transfer reactions, fast ion diffusion kinetics, and stable structures during the charge/discharge process. In other words, MOFs could be used as cathode materials with high energy density, power density and long cycling life.

In order to find more novel MOFs-cathode materials, some researchers paid attention to high valent metal ions as center nodes, such as V(IV), Fe(III), Al(III) and so on. A  $4\text{V K}_{2.5}[(\text{VO})_2(\text{HPO}_4)_{1.5}(\text{PO}_4)_{0.5}(\text{C}_2\text{O}_4)]$  MOF-based cathode has been synthesized by Vittal et al., consisting of a distorted octahedral  $\text{V}^{\text{VO}_6}$  core.  $\text{K}^+$  ions will release upon charging, with subsequent cycles being  $\text{Li}^+$  insertion/extraction from the framework rather than heavier and bigger  $\text{K}^+$ . Besides the ions exchange, V(IV) ions exhibits  $\text{V}^{4+}/\text{V}^{5+}$  redox reaction. The reversible capacities of  $68 \text{ mAh g}^{-1}$  (0.4C),  $58 \text{ mAh g}^{-1}$  (1C),  $40 \text{ mAh g}^{-1}$  (2C) (where  $1\text{C} = 108 \text{ mA g}^{-1}$ ) are obtained between 2.5V and 4.6 V (Vs.  $\text{Li}/\text{Li}^+$ ) after the 60 cycle.<sup>106</sup> In another case,  $\text{Li}_2(\text{VO})_2(\text{HPO}_4)_2(\text{C}_2\text{O}_4)$ , with  $\text{Li}^+$  ion intercalation and  $\text{V}^{4+}/\text{V}^{5+}$  redox reaction during the charge/discharge process presents the charge/discharge capacities of  $83/80 \text{ mAh g}^{-1}$  at 25<sup>th</sup> cycle together with a CE of 97% at 0.1C ( $1\text{C} = 125 \text{ mA g}^{-1}$ ) between 2.5V and 4.5V (vs.  $\text{Li}/\text{Li}^+$ ).<sup>107</sup> MIL-47 (V), with the formula of  $[\text{V}^{\text{IV}}(\text{O})(\text{bdc})]$ , which is able to display a capacity of  $82 \text{ mAh g}^{-1}$  accompanied with  $\sim 100\%$  CE at  $10 \text{ mA g}^{-1}$  between 1.5-4.0V (Vs.  $\text{Li}/\text{Li}^+$ ).<sup>105</sup>  $\text{NCHU-3}$ ,  $[\text{Ga}_2(\text{VO})_3\text{K}_2(\text{H}_2\text{O})_3(\text{C}_2\text{H}_4\text{P}_2\text{O}_6)_4(\text{H}_2\text{O})_{13}]$ , featuring redox oxovanadyl centers, demonstrates a stable cyclability over 200 cycles at the voltage of 3-5V.<sup>222</sup> In addition, Fe<sup>III</sup>-based MOFs, including MIL-101, MIL-100 and MIL-53, can uptake  $\sim 0.62 \text{ Li}$  ions or  $\text{Na}$  ions per Fe nodes above 1.5V (Vs.  $\text{Li}/\text{Li}^+$ ,  $\text{Na}/\text{Na}^+$ ). Yamada et al. proposed the usage of MIL-101(Fe) cathodes, observing a discharge capacity of  $107 \text{ mAh g}^{-1}$  during 2.0-4.2 V at 0.02C and a stable capacity of  $72 \text{ mAh g}^{-1}$  on 100<sup>th</sup> cycles at 0.2C.<sup>223</sup> Tarascon et al. chose MIL-53 (Fe) as a cathode candidate with specific capacity of  $75 \text{ mAh g}^{-1}$  and  $140 \text{ mAh L}^{-1}$  between 1.5V and 3.5 V (Vs.  $\text{Li}/\text{Li}^+$ ) at 0.025C, ascribing to the reversible redox reaction of  $\text{Fe}^{\text{III}}/\text{Fe}^{\text{II}}$  as well as the insertion/extraction of  $\text{Li}^+$  ions.<sup>98</sup> Gallis et al. investigated the positive electrode performance of MIL-100 (Fe) cathodes for sodium ion storage, showing the best performance at 1 M  $\text{NaClO}_4$  in EC: PC: DME. The initial capacity of about  $55 \text{ mAh g}^{-1}$  during 1.5-4.0 V (Vs.

$\text{Na}/\text{Na}^+$ ) at a 0.1C is obtained, which equals to about  $0.6 \text{ Na}/\text{Fe}$  and near to the intercalation of other Fe-MOFs in LIBs.<sup>170</sup> What's more, Lee et al. firstly introduced P(THBQ-Al) coordination polymers (THBQ= tetrahydroxybenzoquinone) into sodium-ion batteries as the cathode, resulting in a specific capacity of  $\sim 113 \text{ mAh g}^{-1}$  at  $20 \text{ mA g}^{-1}$  among 1.5-3V (Vs.  $\text{Na}/\text{Na}^+$ ) and maintaining a stable capacity over 100 cycles.<sup>179</sup> Additionally, the implantation of disulfide ligand in Cu-MOFs is another strategy to improve the working voltage.<sup>224</sup> The total capacity comes from the reversible cleavage/reformation of the S-S bond on ligands and  $\text{Cu}^{2+}/\text{Cu}^+$  redox reaction in metal nodes, which brings a theoretical value of  $216 \text{ mAh g}^{-1}$  for  $[\text{Cu}(\text{C}_2\text{O}_4)(\text{C}_{10}\text{H}_8\text{N}_2\text{S}_2)]$  without any  $\text{H}_2\text{O}$ . In the experiment, a 2<sup>nd</sup> discharge capacity of  $175 \text{ mAh g}^{-1}$  at the current density of  $50 \text{ mA g}^{-1}$  between 2.4V and 4.1V (Vs.  $\text{Li}/\text{Li}^+$ ) is obtained, and 68% capacity is remained until 50 cycles.

Besides the above-mentioned cathode candidates, the following researches also display excellent positive electrode performance.

$\text{Cu}^{\text{I}}\text{TCNQ}$  (TCNQ=7,7,8,8-tetracyanoquinodimethane) was demonstrated as a cathode material for SIBs for the first time by Huang et al.<sup>180</sup> The reversible reaction, where TCNQ moieties transfer two redox electrons and  $\text{Cu}^{\text{I}}/\text{Cu}^{\text{II}}$  redox couples provide one electron, delivering a theoretical capacity of nearly  $300 \text{ mAh g}^{-1}$ . The electrochemical reaction process of  $\text{CuTCNQ}$  is shown as follows: (1) at the charge process, there is an oxidization of  $\text{Cu}^{\text{I}}\text{TCNQ}/\text{TCNQ}^0 + \text{Cu}^{\text{I}}$  (OCV-3.8V) and  $\text{Cu}^{\text{I}}/\text{Cu}^{\text{II}}$  (3.8-4.1V), (2) at the discharge process, there is a reduction of  $\text{Cu}^{\text{II}}/\text{Cu}^{\text{I}}$  (4.1-3.7V),  $\text{TCNQ}^0 + \text{Cu}^{\text{I}}/\text{Cu}^{\text{I}}\text{TCNQ}$  (3.7-3.0V), and  $\text{Cu}^{\text{I}}\text{TCNQ}/[\text{Cu}^{\text{I}}(\text{TCNQ})_2]^-$  (3.0-2.0V). It is shown that the existence of Cu-N bonds has two functions: (1) to maintain the stability of TCNQ ligands and (2) to improve the redox potential. A specific capacity of  $255 \text{ mAh g}^{-1}$  is obtained at  $20 \text{ mA g}^{-1}$  within 2.0-4.1V (Vs.  $\text{Na}/\text{Na}^+$ ), which approximates to the capacity of a three-electron reaction. When tested at  $50 \text{ mA g}^{-1}$ , it exhibits  $214 \text{ mAh g}^{-1}$  at 1<sup>st</sup> cycles and holds good capacity retention until the 50<sup>th</sup> cycle. Awaga et al. adopted 2,7-anthraquinonedicarboxylic acid as a ligand to fabricate a new MOF-based cathode material,  $[\text{Cu}(2,7\text{-AQDC})(\text{DMF})] \cdot x(\text{DMF})$ .<sup>129</sup> This  $\text{Cu}(2,7\text{-AQDC})$  MOF displays a three-electrons movement during the whole redox reaction and the theoretical capacity is about  $162 \text{ mAh g}^{-1}$ . Its capacity reaches  $147 \text{ mAh g}^{-1}$  at initial cycle and retains at  $\sim 105 \text{ mAh g}^{-1}$  after 50 cycles at  $1 \text{ mA}$  between 1.7V and 4 V (Vs.  $\text{Li}/\text{Li}^+$ ). Long et al. designed a  $\text{Fe}_2(\text{dobpdc})$  MOF, consisting of  $\text{dobpdc}^{4-}$  ligands (= 4,4'-dioxidobiphenyl-3,3'-dicarboxylate) and Fe (II) metal nodes, opening the door to reversibly uptake/release of electrolyte anions.<sup>174</sup> Even though the metal nodes and organic moieties could be oxidized, only the former presents a full reversibility. Interestingly, the insertion of larger anions in the framework endows the cathode with a higher operation potential. It exhibits a stable capacity of  $\sim 90 \text{ mAh g}^{-1}$  after 50 cycles at 1C ( $1\text{C} = 140 \text{ mAh g}^{-1}$ ) between 2.0V and 3.65V (Vs.  $\text{Na}/\text{Na}^+$ ). In addition, Cu-TCA (TCA = tricarboxytriphenyl amine),<sup>128</sup>  $\text{Cd}(\text{II})$ -DPNDI MOFs,<sup>194</sup> and bis(diimino)nickel coordination frameworks<sup>132</sup> have also been applied as LIB electrodes with good electrochemical performance at stable high working voltages.

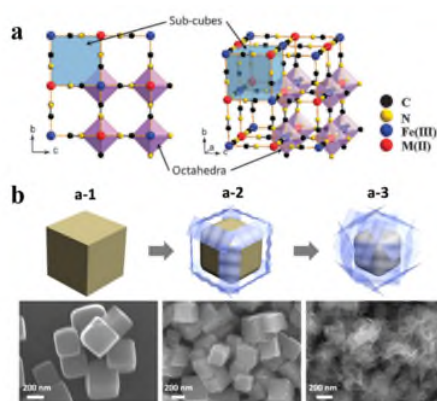


**Fig. 5** (a) The schematic diagram of Prussian blue analogues (PBAs) framework. Reproduced with permission from The Royal Society of Chemistry from ref.230. (b) The scheme of etching methods for a-1-0 h, a-2-0.5 h, a-3-6 h, and the morphology changing from nanocube to nanoflower. Reproduced with permission from ref.231. Copyright 2017 American Chemical Society.

### 3.5 A Particular Family Member of MOPs - PBAs

Prussian blue (PB) and Prussian blue analogous (PBAs) are a large subclass of porous coordination polymers with diverse applications in energy storage devices. As the initially synthesized MOPs, Prussian blue ( $\text{Fe}_4[\text{Fe}(\text{CN})_6]_3 \cdot x\text{H}_2\text{O}$ ) is established by repeating cubic units consisting of mixing-valent  $\text{Fe}^{\text{III}}/\text{Fe}^{\text{II}}$  nodes and cyano ligands.<sup>225</sup> When iron metal ions are replaced by other transitional metal ions, Prussian blue analogous (PBAs) are formed. PB and PBAs, with the general formula of  $\text{A}_x\text{B}_x\text{B}'_y(\text{CN})_6 \cdot n\text{H}_2\text{O}$  ( $\text{A}$ =alkali metal ions,  $\text{B}/\text{B}'$ =transition metal ions), present a fast-ion diffusion kinetics in the solid state, which is contributed from their open hollow frameworks and robust structures. Moreover, for PB and PBAs,  $\text{Li}^+$ ,  $\text{Na}^+$ , and even larger multivalent cations (such as  $\text{K}^+$ ,  $\text{Mg}^{2+}$ ,  $\text{Al}^{3+}$ ), can be reversibly inserted/released and transported through their ion-diffusion channels, in contrast to other inorganic electrode materials.<sup>1</sup> Therefore, the exceptional capability of controllable atomic compositions, peculiar channel structures, and the ability to load different size guest molecules allow PB and PBAs not only to be applied in LIBs and SIBs, but also to be extended to novel battery systems such as K-ions battery, Mg-ions battery, and anion intercalation based-batteries. Some pioneering reports have already reviewed and summarized the PBAs and their derivative nano-materials in energy conversion and storage, including their multi-fold hollow architectures, optimized aqueous and organic electrolyte system, applications in diverse battery system, electrochemical catalysis, and so on.<sup>226-229</sup> Here, recent efforts in the compositional design and structure modification of crystal PBAs will be mainly concluded for sodium-ion batteries and lithium-ion batteries in organic electrolytes.

Since primary electrochemical characteristics of PB batteries have been illuminated by Neff in 1985, PB and its analogues have experienced ever-increasing development in rechargeable batteries.<sup>232-234</sup> Goodenough et al. found that  $\text{KMFe}(\text{CN})_6$  ( $\text{M} = \text{Fe}, \text{Mn}, \text{Ni}, \text{Co}$  and  $\text{Zn}$ ), as shown in Fig. 5a, exhibits a capacity

of  $\sim 100 \text{ mAh g}^{-1}$  at 0.05C during 2.0-4.0 V (Vs.  $\text{Na}/\text{Na}^+$ ) in organic carbonate electrolyte because sodium ions can reversibly intercalate into PBAs accompanying by redox converted  $\text{Fe}^{\text{III}}/\text{Fe}^{\text{II}}$ .<sup>230</sup> Then, they synthesized Na-Mn hexacyanoferrate compounds (NMHFC) with a high redox potential of 3.4V (Vs.  $\text{Na}/\text{Na}^+$ , organic electrolyte).<sup>235</sup> The substitution of sodium ions in iron cyanide complex has a capability to shift the  $\text{Fe}(\text{III})/\text{Fe}(\text{II})$  redox couple to  $\text{Mn}(\text{III})/\text{Mn}(\text{II})$  couple and stabilize more positive charge on Mn ions. Correspondingly, there are  $\text{Fe}(\text{III})/\text{Fe}(\text{II})$  and  $\text{Mn}(\text{III})/\text{Mn}(\text{II})$  redox couples separately located at low and high voltage, as well as reversible  $\text{Na}^+$  uptake/removal during charge/discharge process. So, a reversible capacity of  $\sim 120 \text{ mAh g}^{-1}$  after 30<sup>th</sup> cycles at 1/20C ( $1\text{C}=120 \text{ mA g}^{-1}$ ) within 2-4.2V (Vs.  $\text{Na}/\text{Na}^+$ ) is obtained, indicating that NMHFC is a promising cathode candidate for SIB. After that, Na-rich PBA cathode materials, such as  $\text{Na}_4\text{Fe}(\text{CN})_6$  (2014),  $\text{Na}_2\text{Mn}^{\text{II}}[\text{Mn}^{\text{II}}(\text{CN})_6]$  (2014), Na-rich  $\text{Na}_x\text{FeFe}(\text{CN})_6$  (2015),  $\text{Na}_2\text{CoFe}(\text{CN})_6$  (2018),  $\text{Na}_x\text{M}[\text{Fe}(\text{CN})_6] \cdot n\text{H}_2\text{O}$  ( $\text{M}=\text{Fe}, \text{Mn}, \text{Ni}$ , and  $\text{Co}$ ) (2018) and so on, have become ever-increasingly attractive electrode materials in organic  $\text{Na}^+$  ions battery.<sup>236-240</sup> Besides, the tunability of chemical compositions can also be achieved by developing  $\text{Na}_2\text{Ni}[\text{Fe}(\text{CN})_6]$ ,  $\text{Na}_2\text{VO}_x[\text{Fe}(\text{CN})_6]$ ,  $\text{Zn}_3\text{Na}_2[\text{Fe}^{\text{II}}(\text{CN})_6]_2$ , Cu/Fe PBAs, V/Fe PBAs, Ni-doping  $\text{Na}_4\text{Fe}(\text{CN})_6$ , etc.<sup>162, 241-247</sup> Interestingly, Han et al. prepared novel PBAs- $\text{Ni}_x\text{Co}_{1-x}[\text{Fe}(\text{CN})_6]$  ( $x=0, 0.1, 0.2, \dots, 1.0$ ) and developed them in a full cell with an anode material  $\text{NaTi}_2(\text{PO}_4)_3$  (NTP).<sup>248</sup> The full-cell performance of HQ-NiCoFe ( $x=0.3$ )/NTP exhibits a practical specific capacity of  $\sim 140 \text{ mAh g}^{-1}$  at  $15 \text{ mA g}^{-1}$  between 0.5V and 2.2 V, which is close to the theoretical capacity of  $145 \text{ mAh g}^{-1}$  (1.68 Na per units), a good capacity retention, and  $\sim 100\%$  CE after 300 cycles at  $150 \text{ mA g}^{-1}$ . During the sodiation/desodiation process, there are reversible  $\text{Fe}^{2+}/\text{Fe}^{3+}$  and  $\text{Co}^{2+}/\text{Co}^{3+}$  redox reactions for inputting/outputting electrons, suggesting the presence of redox innocent Ni in PBAs. The great electrochemical performance of HQ- $\text{Ni}_{0.3}\text{Co}_{0.7}[\text{Fe}(\text{CN})_6]$  results from two aspects: (1) the introduction of inactive Ni enables to reduce lattice variation and then cure capacity recession, and (2) fewer  $\text{Fe}(\text{CN})_6$  vacancies and  $\text{H}_2\text{O}$  in HQ-PBA frameworks. One of the effective post-treatment approaches to tailor PBAs' morphology and active  $\text{Na}^+$  storage sites is via the tunable etching methods by selectively adding NaOH or HCl in PBAs solution.<sup>249-251</sup> Mai et al. proposed a defect-induced mechanism that stimulates the morphology changing from nanocube to nanoflower through dispersing pristine  $\text{Na}_x\text{NiFe}(\text{CN})_6$  nanocubes into NaOH solution, followed by sonication (Fig. 5b).<sup>249</sup> During the extended etching process along each face, the edges of NiHCF-cubes gradually dissolve and recrystallize. Finally, the nanocubes are transformed into nanosheets and then nanoflowers. Meanwhile,  $\sim 300 \text{ nm}$  bulk NiHCF-cubes are reduced into  $100\text{-}200 \text{ nm}$  internal cubes. At the rate of 1.1C ( $1\text{C}=90 \text{ mA g}^{-1}$ ) within 2.0-4.0V (Vs.  $\text{Na}/\text{Na}^+$ ), the 2<sup>nd</sup> cycle capacity of NiHCF-etch ( $1.0 \text{ Na/f.u.}$ ,  $\sim 90 \text{ mAh g}^{-1}$ ) is higher than that of NiHCF-cube ( $0.73 \text{ Na/f.u.}$ ,  $\sim 66 \text{ mAh g}^{-1}$ ). Additionally, the capacity retention rate after 5000 cycles at 5.5C of the NiHCF-etch and NiHCF-cube are  $\sim 83.2\%$  and  $\sim 76.9\%$ , respectively. The above data reveals that post-etching treatment can be effective, in other words, the sodium-ion diffusion kinetics of

optimized nanoflower NiHCF-etch samples is faster than that of original NiHCF-cubes during the process of sodiation/desodiation. What's more, adding PVP in etching solution that will adjust the size distribution of PBAs by controlling the etching rate,<sup>251</sup> mixing ascorbic acid and acetic acid in PBAs solution under a certain heat treatment that will fabricate hierarchical hollow architecture,<sup>252</sup> inhibitor control that will prepare a border-rich structure,<sup>253</sup> and other strategies<sup>254, 255</sup> have been verified and could guide future research.<sup>256</sup>

Attractively, PBAs also feature a high lithium insertion/extraction voltage ( $\sim 3$  V vs. Li/Li<sup>+</sup>, organic electrolyte), inspiring people to explore and improve its LIBs performance.<sup>257</sup> Yang et al. reported nanocubic FeFe(CN)<sub>6</sub> crystals with well-arranged lattice defects, demonstrating a high specific capacity of 160 mAh g<sup>-1</sup> (about 1.8 Li<sup>+</sup> ions per units) and an energy density of about 500 Wh kg<sup>-1</sup> at 0.15 C (1 C = 160 mA g<sup>-1</sup>) within 2.0–4.3 V (vs. Li/Li<sup>+</sup>), a capacity value of 102 mAh g<sup>-1</sup> at a very high rate of 24C (up to  $\sim 3840$  mA g<sup>-1</sup>), and a stable long cycling life over 300 cycles with 90% capacity retention at 3C.<sup>258</sup> Long et al. has shown a Tb(H<sub>2</sub>O)<sub>5</sub>[W(CN)<sub>8</sub>] coordination polymer as lithium storage cathodes between 2.5V and 4.3 V (vs. Li/Li<sup>+</sup>), with redox couples of [W<sup>V</sup>(CN)<sub>8</sub>]<sup>3-</sup>/[W<sup>IV</sup>(CN)<sub>8</sub>]<sup>4-</sup> at 3.3 V and  $\sim 70\%$  reversible Li<sup>+</sup> intercalation at initial cycle.<sup>259</sup> Yagi et al. quantitatively reveals the redox active intercalation of PF<sub>6</sub><sup>-</sup> anions and Li<sup>+</sup> cations in a PB battery.<sup>260</sup> Talham et al. investigated a core-shell structure CuFe-PBA@NiFe-PBA as cathodes in LIB accompanied with a stepwise redox reaction of Fe<sup>3+/2+</sup> (CuFe-PBA), Fe<sup>3+/2+</sup> (NiFe-PBA), and Cu<sup>2+/+</sup> (CuFe-PBA).<sup>261</sup> Apart from as the positive electrodes, PBAs still present excellent negative-electrode performance in LIBs.<sup>262–265</sup> In conclusion, PBAs-related electrode materials bring an interesting and broad realm of battery chemistry. This section may provide some practical strategies for further advanced research to boost more remarkable charge/discharge performance.

### 3.6 Other Approaches

Several main strategies for enhancing the electrochemical performance of MOPs materials have been summarized at above-mentioned contents. Rational design and fabrication of MOPs materials basically take the metal centers and bridging segments into account in order to prepare extraordinary electrode candidates with thermal/chemical consistency, electric/ionic conductivity, high operation voltage, and multiple redox-active sites. Furthermore, an overall consideration could be taken toward multi-dimensional porous structures, particle size, various morphologies, and so on. The porous channels of MOPs are important transfer pathways for mobile protons or ions.<sup>16</sup> When talking about the pore structures among MOPs frameworks, the pore radius size, pore shapes, and whether guest molecules occupy the pores, are three issues, which need to be addressed.<sup>94, 105, 266</sup> Meanwhile, multi-dimensional MOPs, which could be regulated through controlling the crystal growth direction, are another focus when designing the whole structures.<sup>267</sup> Comparing with 1D particles<sup>87, 268</sup> and 3D porous

frameworks, 2D layers structure have become increasingly attractive in recent works.<sup>14, 69, 90–92, 123–124</sup> 2D layer-by-layer deposited nanosheets, usually featuring with ultra-thin thickness and ultra-high specific areas, are able to offer numerous accessible reactive sites and have the potential to manufacture electrically conductive networks.<sup>14, 269</sup> Furthermore, conventional 2D conductive materials, such as graphene, are restricted by their component elements and difficulty in proceeding post-modification, while 2D conductive MOPs materials are charming because of the diversity in their composition and easy tailoring.<sup>197</sup>

It is feasible to control the nanosized particles and their morphologies by adjusting synthetic conditions.<sup>15</sup> The controlled nano-particles and morphologies directly influence the contact interfaces between electrodes and electrolyte, which shortens electron/charge diffusion distance and hence decides the rate of electrochemical reaction.<sup>223, 270</sup> Xu et al. reported sub-5nm Co-MOF crystals pulverized from bulk particles by coating protective PPy and subsequent calcination treatment (Fig. 6a).<sup>212</sup> The ultrasmall nanocrystals crucially

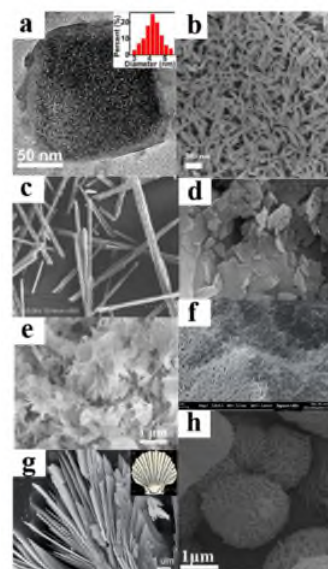


**Fig. 6** TEM and SEM images of (a) sub-5 nm nanoparticle of Co-MOF, the size distribution is inserted. Reproduced with permission from ref.212. Copyright 2018 American Chemical Society. (b) Nanorods of Fe-MIL-88B. Reproduced with permission from ref.167. Copyright 2017 Elsevier. (c) Needle of Fe PCN-600 MOFs. [ref.181]-Reproduced by permission of The Royal Society of Chemistry. (d) Nanosheets of u-CoOHtp MOFs. Reproduced with permission from ref.124. Copyright 2018 Elsevier. (e) Microflowers of H-Co-MOF. Reproduced with permission from ref.113. Copyright 2018 Wiley-VCH Verlag GmbH & Co. KGaA. (f) Nanowires of Co-CPs. Reproduced from ref.93 with permission from The Royal Society of Chemistry. (g) Seashell-like S-Co-MOF. Reproduced from ref.95 with permission from The Royal Society of Chemistry (h) Honeycomb-like Zn/Ni-MOF. Reproduced with permission from ref.160. Copyright 2018 Elsevier.

increase the solid/liquid interface areas and especially improve their fast charge/discharge ability at high current rate. At 0.2A g<sup>-1</sup> among 0.01-3 V (Li/Li<sup>+</sup>), the 2<sup>nd</sup> cycle capacity is 1201 mAh g<sup>-1</sup> with CE of over 95%, and the 100<sup>th</sup> cycle stables at 1192 mAh g<sup>-1</sup> with CE of about 99%. It also obtains an excellent rate capability as shown in their high capacities of 1301 mAh g<sup>-1</sup> (0.1 A g<sup>-1</sup>), 1188 mAh g<sup>-1</sup> (0.2 A g<sup>-1</sup>), 1060 mAh g<sup>-1</sup> (0.5 A g<sup>-1</sup>), 987 mAh g<sup>-1</sup> (1 A g<sup>-1</sup>), 906 mAh g<sup>-1</sup> (2 A g<sup>-1</sup>), 801 mAh g<sup>-1</sup> (5 A g<sup>-1</sup>), 701 mAh g<sup>-1</sup> (10 A g<sup>-1</sup>), and 596 mAh g<sup>-1</sup> (20 A g<sup>-1</sup>).

Special morphology-dependent synthetic routes are substantially allied with subsequent specific capacity test and cycling performance.<sup>85</sup> Up to now, MOPs have been demonstrated to show varied morphologies and distinguished battery performance. From nanorods (Fe-MIL-88B (Fig. 6b),<sup>167</sup> CoHNta CPs),<sup>187</sup> needle (Fe PCN-600 MOFs (Fig. 6c)),<sup>181</sup> nanosheets (Co<sup>II</sup>-terephthalate-based MOF (Fig. 6d)),<sup>124</sup> nanowires (Co-CPs (Fig. 6f)),<sup>93</sup> pillared (Mn<sup>II</sup> and Co<sup>II</sup>-MOFs),<sup>195</sup> 271 ellipsoids (Ni<sub>3</sub>(HCOO)<sub>6</sub>/CNTs),<sup>176</sup> tremella-like (Al-fumarate based MOFs),<sup>140</sup> to more complicated appearances such as honeycomblike Zn/Ni-MOF (Fig. 6h)<sup>160</sup> and flower-like Ni(BTC) MOFs,<sup>109</sup> all have been confirmed to display the valid effects of smart morphology adjustment. Apart from the accommodating salt concentrations and the as-treated temperatures, porous carbon materials (graphene and CNTs) also have been used as templates for the growth of specific shapes to enhance Li<sup>+</sup>/Na<sup>+</sup> storage capacity.<sup>108, 207</sup> An interesting morphology evolution toward Co-BDC MOFs has been reported by different groups, confirming that the modified morphology is helpful for improving electrode performance. For example, Li et al. synthesized Co<sub>2</sub>(OH)<sub>2</sub>BDC MOFs with large bulk grain structure, exhibiting 100<sup>th</sup> capacity of ~650 mAh g<sup>-1</sup> at 50 mA g<sup>-1</sup> between 0.02V and 3.0 V (Li/Li<sup>+</sup>). In a following work, Hu et al. prepared seashell-like Co<sub>2</sub>(OH)<sub>2</sub>BDC MOFs and employed it as a LIB anode (0.01-3.0 V) (Fig. 6g).<sup>95</sup> The hierarchical seashell-like structure has two merits: (1) containing many cavities inside for storing more electrolyte, and (2) decreasing ion diffusion resistance because of the high contacting specific surfaces. The 200<sup>th</sup> cycle capacity of 1021 mAh g<sup>-1</sup>, 700<sup>th</sup> cycle capacity of 601 mAh g<sup>-1</sup> and 1000<sup>th</sup> cycles capacity of 435 mAh g<sup>-1</sup> are obtained at 100 mA g<sup>-1</sup>, 500 mA g<sup>-1</sup> and 1 A g<sup>-1</sup>, respectively, showing stable ultra-long cyclability and high-rate discharge ability. In the same year, they also reported shale-shaped Co(1,4-BDC)(DMF)<sub>0.61</sub> MOFs microcrystals, which display a 100<sup>th</sup> cycle capacity of 1090.2 mAh g<sup>-1</sup> at 200 mA g<sup>-1</sup> and 200<sup>th</sup> cycle capacity of 611 mAh g<sup>-1</sup> at 1000 mA g<sup>-1</sup> among 0.01-3.0 V (Vs. Li/Li<sup>+</sup>). More recently, Wei et al. presented hierarchical Co<sub>2</sub>(OH)<sub>2</sub>BDC microflowers (formed by aggregating many small nanoflakes) (Fig. 6e), and tested them as anodes for LIBs (0.01-3.0V).<sup>113</sup> Owing to their unique microflower morphologies and high specific areas, the lithium storage capacity could reach up to 1345 mAh g<sup>-1</sup> at 0.1 A g<sup>-1</sup> after 100 cycles, and 828 mAh g<sup>-1</sup> at 2 A g<sup>-1</sup> after 700 cycles.

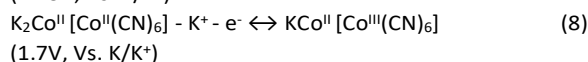
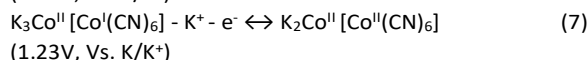
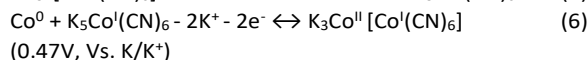
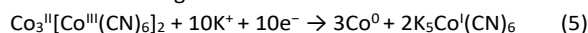
#### 4. Promotion of Other Advanced Applications

As the diverse energy storage and conversion devices developed so far, pristine MOFs and CPs have been used as active elements in many promising systems, such as Li-S

batteries, Li-O<sub>2</sub> battery, solar cells, fuel cells, supercapacitors and so on.<sup>13, 64, 65, 200, 218, 272-280</sup> Early reviews have already summarized several of these emerging applications. Here, the development of other cations-based batteries (K<sup>+</sup>, Zn<sup>2+</sup>, Mg<sup>2+</sup>) will be typically highlighted.

The reason for alternating traditional graphite anodes comes from its low gravimetric capacity (372 mAh·g<sup>-1</sup>), poor rate performance and unable to accommodate larger ions than Li<sup>+</sup>/Na<sup>+</sup> while maintain intact structure. However, CPs (particularly PBAs) hold great advantages in accommodating various cations via their unique nanopores and cross-linked channels.<sup>18, 281-288</sup> Most importantly, they are facile to be produced and low cost.<sup>289</sup>

First is mono-valent K<sup>+</sup> ion batteries. An organic K<sup>+</sup> ion battery, based on a typical PBA-Co<sub>3</sub>[Co(CN)<sub>6</sub>]<sub>2</sub> anode, is reported and found with a favorable performance of 324.5 mAh g<sup>-1</sup> at 100 mA g<sup>-1</sup> among 0.05-2 V (Vs. K/K<sup>+</sup>) and ~82% capacity retention rate after 200 cycles.<sup>290</sup> A rate capacity of 221 mAh g<sup>-1</sup> is also obtained at the high current density of 1000 mA g<sup>-1</sup>. This significant work reveals a multistep potassiation/depotassiation process at C-Co and N-Co redox active sites, which is controlled by solid-state diffusion. An initial irreversible K<sup>+</sup> insertion step and subsequent reversible K<sup>+</sup> uptake/removal process are shown as following:



(1.7V, Vs. K/K<sup>+</sup>) Therefore, eight mole electrons per unit could be offered among reaction (6), (7) and (8), and the value of theoretic capacity is up to 354 mAh g<sup>-1</sup>. With regard to organic KIB cathodes, Goodenough et al. also proposed to use K<sub>x</sub>MnFe(CN)<sub>6</sub> (0 ≤ x ≤ 2) for storing K<sup>+</sup> ions at 3.6V working plateaus via two redox couples such as Mn<sup>III</sup>/Mn<sup>II</sup> or Fe<sup>III</sup>/Fe<sup>II</sup>.<sup>291</sup> This PBA-based cathode presents a discharge capacity of 142.4 mAh g<sup>-1</sup> at rate of 0.2 C within 2.5-4.6V (Vs. K/K<sup>+</sup>), close to its theoretical capacity of ~156 mAh g<sup>-1</sup> (about 2 K<sup>+</sup> per unit).

Secondly, multivalent-cation batteries show the merits of abundant conservation on earth, ultra-safety and high energy density (e.g. the theoretical gravimetric and volumetric capacity of Mg metal anode could reach 2205 Ah kg<sup>-1</sup> and 3833 mAh cm<sup>-3</sup>, respectively). They have been broadly widened the usage in aqueous electrolyte and organic electrolyte after the introduction of chemically/thermally stable CPs (PBAs).<sup>292-295</sup> To avoid the inert phase conversion at Mg metal surfaces and improve the ion diffusion kinetics at both side of the electrodes, an MgSO<sub>4</sub>-based aqueous electrolyte accompanying with polyimide anode and PBAs cathodes are designed and fabricated to realize magnesium-ion storage via reversible enolization at negative polyimide electrodes and Mg<sup>2+</sup> insertion/extraction at positive PBAs electrodes.<sup>296</sup> This full aqueous Mg ions battery takes energy density of about 33 Wh kg<sup>-1</sup>, closing to theoretical capacity of 48 Wh kg<sup>-1</sup>, at 1 A g<sup>-1</sup> among 0-1.55 V (Vs. Mg/Mg<sup>2+</sup>), and ~100% capacity retention

after 100 cycles at 2 A g<sup>-1</sup>. However, suffered from the limited windows (~1.2V), non-redox active ions intercalation (protons

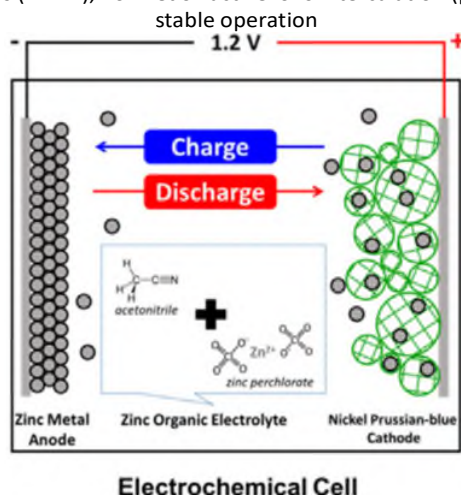


**Fig. 7** The charge/discharge principle of organic Mg-ions battery based on KNF-086 PBAs cathode and Zinc metal anode. Reproduced with permission from ref.297. Copyright 2016 Elsevier.

and H<sub>3</sub>O<sup>+</sup>), negative metal corrosion in acid electrolyte and the formation of insulated ZnO layers, so aqueous electrolyte systems of zinc ions battery cannot avoid low utilization of Zn ions, poor cyclability, and low discharge capacity/charge capacity rate (CE). In order to address these issues, Hong et al. studied an organic electrolyte (0.5M Zn(ClO<sub>4</sub>)<sub>2</sub> in acetonitrile solvent) for rechargeable Zn ions battery, where KNF-086 PBAs are used as positive electrodes (Fig. 7).<sup>297</sup> It is revealed that Zn<sup>2+</sup> ions are inserted into the interstitial cavities of PBA crystal, delivering an initial capacity of 55.6 mAh g<sup>-1</sup> at rate 0.2 C (1C= 56 mA g<sup>-1</sup>) within 0.7–1.8V (Vs. Zn/Zn<sup>2+</sup>) and high CE of over 99.9%. Indeed, PBA-based electrode is not prerequisite in organic multivalent-cations batteries. For example, α-Mo<sub>3</sub>S<sub>11</sub> CP also exhibits the ability of reversible magnesiation/demagnesiation at the terminal redox active S-S moieties, displaying a discharge capacity of 115 mAh g<sup>-1</sup> at 1<sup>st</sup> cycle at 10 mA g<sup>-1</sup> among 0.2–2.2 V (Vs. Mg/Mg<sup>2+</sup>).<sup>298</sup>

## 5. Summary and Outlook

MOPs (CPs, MOFs, PB and PBAs) are promising alternatives with the enhanced energy density and reduced cost to replace conventional intercalated materials. The availability of wide operation voltage range (0.01–4.5V) and high specific capacity makes them powerful to compete with commercial electrode materials such as lithium iron phosphate (3.4 V, 170 mAh g<sup>-1</sup>) and lithium cobalt oxide (4 V, 140 mAh g<sup>-1</sup>).<sup>291</sup> In this review, we have discussed the types of redox reactions and electrochemical mechanisms of MOPs during the ion insertion/extraction: (1) insertion-type MOPs with redox-active bridging linkers or both redox-active metal ions and ligands are recommended to be electrodes with the best performance, and (2) novel “bipolar charging” principle could be beneficial for further study of varied-size cations/anions intercalation. Moreover, feasible strategies including: (1) chemical

modification toward both inorganic metal nodes and organic linkers, (2) careful refinement of high working potential cathode substitutes and preeminent PBAs candidates, and (3) morphology tuning, have been proposed in this review to design novel MOPs-based electrode materials for superior battery performance. The bottleneck of pristine MOPs in EES applications is their insulating property. Fortunately, the electrical conductivity of MOPs could be improved by employing 2D π - π stacking nanosheets structure, wherein the delocalized electron cloud could be located at π - conjugated in-plane and interlayers. Therefore, constructing 2D π - π conjugated inter-layers structure from plane ligands and transitional metal ions is a good suggestion to overcome the intrinsic insulation behavior of MOPs. Additionally, MOPs with unique porosity and ordered channel distributions are suitable electrode materials for rechargeable batteries based on large-sized cation intercalation mechanism. However, to date, there are still many challenges for MOPs. Great efforts should be made in the following ways: (1) simpler and mass-production synthetic routes are required to be proposed for the development of cheap materials; (2) The improved conductivity and structure stability of pristine MOPs must be engineered to achieve excellent rate capability and long-life cyclability; and (3) More EES devices should be fabricated with the use of diverse MOPs materials. By reviewing the current situation of MOPs materials in sustainable EES technology, we believe that more breakthroughs in EES-related applications would be achieved for satisfying the rapidly-growing demand of high-performance portable energy storage systems.

## Conflicts of interest

There are no conflicts to declare.

## Acknowledgements

Q.Z. acknowledges financial support from AcRF Tier 1 (RG 111/17, RG 2/17, RG 114/16, RG 8/16) and Tier 2 (MOE 2017-T2-1-021 and MOE 2018-T2-1-070), Singapore. S.Z. acknowledges financial support from Australia Research Council Discovery projects (DP170103721 and DP180102003).

## Notes and references

- 1 H. B. Wu and X. W. D. Lou, *Sci Adv*, 2017, **3**, 9252.
- 2 Y. Q. Zhang, X. Liu, S. L. Wang, L. Li and S. X. Dou, *Adv. Energy Mater.*, 2017, **7**, 1700592.
- 3 T. Z. Yang, T. Qian, M. F. Wang, X. W. Shen, N. Xu, Z. Z. Sun and C. L. Yan, *Adv. Mater.*, 2016, **28**, 539–545.
- 4 A. M. Abioye and F. N. Ani, *Renew. Sust. Energy Rev.*, 2015, **52**, 1282–1293.
- 5 Y. Q. Zhang, X. Liu, S. L. Wang, S. X. Dou and L. Li, *J. Mater. Chem. A*, 2016, **4**, 10869–10877.
- 6 (a) J. Lu, Z. H. Chen, Z. F. Ma, F. Pan, L. A. Curtiss and K. Amine, *Nat. Nanotechnol.*, 2017, **12**, 90–90. (b) Y. L. Liang and Y. Yao, *Joule*, 2018, **2**, 1690–1706.
- 7 (a) J. Xie and Q. Zhang, *J. Mater. Chem. A*, 2016, **4**, 7091–7106; (b) J. Wu, X. Rui, C. Wang, W.-B. Pei, R. Lau, Q. Yan and Q. Zhang, *Adv. Energy Mater.*, 2015, **5**, 1402189; (c) J. Xie, P.

- Gu and Q. Zhang, *ACS Energy Lett.*, 2017, **2**, 1985–1996; (d) Z.-Q. Lin, J. Xie, B. Zhang, J. Li, J.-N. Weng, R.-B. Song, X. Huang, H. Zhang, H. Li, Y. Liu, Z. J. Xu, W. Huang and Q. Zhang, *Nano Energy*, 2017, **41**, 117–127; (e) J. Xie, W. Chen, Z. Wang, K. C. W. Jie, M. Liu and Q. Zhang, *Chem Asian J.*, 2017, **12**, 868–876; (f) J. Xie, Z. Wang, Z. J. Xu and Q. Zhang, *Adv. Energy Mater.*, 2018, **8**, 1703509; (g) J. Xie, W. Chen, G. Long, W. Gao, Z. J. Xu, M. Liu and Q. Zhang, *J. Mater. Chem. A*, 2018, **6**, 12985 – 12991; (h) J. Xie, C.-E. Zhao, Z. Lin, P.-Y. Gu, Q. Zhang, *Chem. Asian J.*, 2016, **11**, 1489–1511.
- 8 S. Kajiyama, L. Szabova, K. Sodeyama, H. Iinuma, R. Morita, K. Gotoh, Y. Tateyama, M. Okubo and A. Yamada, *Acs Nano*, 2016, **10**, 3334–3341.
- 9 Y. Q. Zhang, Q. Ma, S. L. Wang, X. Liu and L. Li, *Acs Nano*, 2018, **12**, 4824–4834.
- 10 M. S. Balogun, Y. Luo, W. T. Qiu, P. Liu and Y. X. Tong, *Carbon*, 2016, **98**, 162–178.
- 11 Y. Wu and Y. Yu, *Energy Storage Mater.*, 2019, **16**, 323–343.
- 12 H. L. Zhang, H. B. Zhao, M. A. Khan, W. W. Zou, J. Q. Xu, L. Zhang and J. J. Zhang, *J. Mater. Chem. A*, 2018, **6**, 20564–20620.
- 13 X. Zhang, A. Chen, M. Zhong, Z. Zhang, X. Zhang, Z. Zhou and X.-H. Bu, *Electrochemical Energy Rev.*, 2018, 1–76.
- 14 J. D. Sosa, T. F. Bennett, K. J. Nelms, B. M. Liu, R. C. Tovar and Y. Y. Liu, *Crystals*, 2018, **8**, 325.
- 15 Z. B. Liang, C. Qu, W. H. Guo, R. Q. Zou and Q. Xu, *Adv. Mater.*, 2018, **30**, 39.
- 16 F. Y. Yi, R. Zhang, H. L. Wang, L. F. Chen, L. Han, H. L. Jiang and Q. Xu, *Small Methods*, 2017, **1**, 1700187.
- 17 J. W. Zhou and B. Wang, *Chem. Soc. Rev.*, 2017, **46**, 6927–6945.
- 18 Z. Y. Zhang and K. Awaga, *Mrs Bull.*, 2016, **41**, 883–889.
- 19 H. B. Zhang, J. W. Nai, L. Yu and X. W. Lou, *Joule*, 2017, **1**, 77–107.
- 20 J. W. Ren, M. Ledwaba, N. M. Musyoka, H. W. Langan, M. Mathe, S. J. Liao and W. Pang, *Coord. Chem. Rev.*, 2017, **349**, 169–197.
- 21 H. L. Wang, Q. L. Zhu, R. Q. Zou and Q. Xu, *Chem*, 2017, **2**, 52–80.
- 22 Y. Zhao, Z. X. Song, X. Li, Q. Sun, N. C. Cheng, S. Lawes and X. L. Sun, *Energy Storage Mater.*, 2016, **2**, 35–62.
- 23 (a) S. R. Batten, N. R. Champness, X. M. Chen, J. Garcia-Martinez, S. Kitagawa, L. Ohrstrom, M. O'Keeffe, M. P. Suh and J. Reedijk, *Crystengcomm*, 2012, **14**, 3001–3004. (b) K. Biradha, A. Ramana and J. J. Vittal, *Cryst. Growth Des.*, 2009, **9**, 2969–2970.
- 24 (a) J. Zhao, W.-W. Dong, Y.-P. Wu, Y.-N. Wang, C. Wang, D.-S. Li and Q. Zhang, *J. Mater. Chem. A*, 2015, **3**, 6962–6969; (b) J. Gao, M. He, Z. Y. Lee, W. Cao, W. W. Xiong, Y. Li, R. Ganguly, T. Wu and Q. Zhang, *Dalton Transactions*, 2013, **42**, 11367 – 11370; (c) J. Zhao, Y. Wang, W. Dong, Y. Wu, D. Li, B. Liu, and Q. Zhang, *Chem Comm.* 2015, **51**, 9479–9482.
- 25 (a) H. C. Zhou, J. R. Long and O. M. Yaghi, *Chem. Rev.*, 2012, **112**, 673–674. (b) S. R. Batten and N. R. Champness, *Philos. Trans. R. Soc. A-Math. Phys. Eng. Sci.*, 2017, **375**, 4.
- 26 (a) G.-W. Xu, Y.-P. Wu, W.-W. Dong, J. Zhao, X.-Q. Wu, D.-S. Li and Q. Zhang, *Small*, 2017, **13**, 160299; (b) J. Gao, L. Bai, Q. Zhang, Y. Li, G. Rakesh, J.-M. Lee, Y. Yang and Q. Zhang, *Dalton Transactions*, 2014, **43**, 2559 – 2565; (c) Y.-P. Wu, X.-Q. Wu, J.-F. Wang, J. Zhao, W.-W. Dong, D.-S. Li and Q. Zhang, *Crystal Growth & Design*, 2016, **16**, 2309–2316.
- 27 (a) H. Furukawa, K. E. Cordova, M. O'Keeffe and O. M. Yaghi, *Science*, 2013, **341**, 1230444. (b) C. S. Vogelsberg and M. A. Garcia-Garibay, *Chem. Soc. Rev.*, 2012, **41**, 1892–1910.
- 28 (a) P. Li, F.-F. Cheng, W.-W. Xiong and Q. Zhang, *Inorg. Chem. Front.* 2018, **5**, 2693 – 2708; (b) X. Zhan, Z. Chen, Q. Zhang, *J. Mater. Chem. A.*, 2017, **5**, 14463 – 14479.
- 29 M. Rubio-Martinez, C. Avci-Camur, A. W. Thornton, I. Imaz, D. Maspoch and M. R. Hill, *Chem. Soc. Rev.*, 2017, **46**, 3453–3480.
- 30 H. Y. Guan, R. J. LeBlanc, S. Y. Xie and Y. F. Yue, *Coord. Chem. Rev.*, 2018, **369**, 76–90.
- 31 E. Barea, C. Montoro and J. A. R. Navarro, *Chem. Soc. Rev.*, 2014, **43**, 5419–5430.
- 32 E. Jeong, W. R. Lee, D. W. Ryu, Y. Kim, W. J. Phang, E. K. Koh and C. S. Hong, *Chem. Commun.*, 2013, **49**, 2329–2331.
- 33 R. Banerjee, H. Furukawa, D. Britt, C. Knobler, M. O'Keeffe and O. M. Yaghi, *J. Am. Chem. Soc.*, 2009, **131**, 3875–3877.
- 34 J. N. Hao and B. Yan, *Chem. Commun.*, 2015, **51**, 7737–7740.
- 35 E. Tahmasebi, M. Y. Masoomi, Y. Yamini and A. Morsali, *Inorg. Chem.*, 2015, **54**, 425–433.
- 36 Y. J. Zhang, Z. Q. Xie, Z. Q. Wang, X. H. Feng, Y. Wang and A. G. Wu, *Dalton Trans.*, 2016, **45**, 12653–12660.
- 37 N. A. Khan, Z. Hasan and S. H. Jhung, *J. Hazard. Mater.*, 2013, **244**, 444–456.
- 38 A. C. McKinlay, R. E. Morris, P. Horcajada, G. Ferey, R. Gref, P. Couvreur and C. Serre, *Angew. Chem.-Int. Edit.*, 2010, **49**, 6260–6266.
- 39 L. E. Kreno, K. Leong, O. K. Farha, M. Allendorf, R. P. Van Duyne and J. T. Hupp, *Chem. Rev.*, 2012, **112**, 1105–1125.
- 40 V. Stavila, A. A. Talin and M. D. Allendorf, *Chem. Soc. Rev.*, 2014, **43**, 5994–6010.
- 41 P. Kumar, A. Deep and K. H. Kim, *Trac-Trends Anal. Chem.*, 2015, **73**, 39–53.
- 42 J. P. Lei, R. C. Qian, P. H. Ling, L. Cui and H. X. Ju, *Trac-Trends Anal. Chem.*, 2014, **58**, 71–78.
- 43 H. B. Zhang, G. G. Liu, L. Shi, H. M. Liu, T. Wang and J. H. Ye, *Nano Energy*, 2016, **22**, 149–168.
- 44 M. A. Nasalevich, M. van der Veen, F. Kapteijn and J. Gascon, *Crystengcomm*, 2014, **16**, 4919–4926.
- 45 C. A. Downes and S. C. Marinescu, *ChemSusChem*, 2017, **10**, 4374–4392.
- 46 S. L. Zhao, Y. Wang, J. C. Dong, C. T. He, H. J. Yin, P. F. An, K. Zhao, X. F. Zhang, C. Gao, L. J. Zhang, J. W. Lv, J. X. Wang, J. Q. Zhang, A. M. Khattak, N. A. Khan, Z. X. Wei, J. Zhang, S. Q. Liu, H. J. Zhao and Z. Y. Tang, *Nat. Energy*, 2016, **1**, 16184.
- 47 E. M. Miner, T. Fukushima, D. Sheberla, L. Sun, Y. Surendranath and M. Dinca, *Nat. Commun.*, 2016, **7**, 10942.
- 48 A. J. Clough, J. W. Yoo, M. H. Mecklenburg and S. C. Marinescu, *J. Am. Chem. Soc.*, 2015, **137**, 118–121.
- 49 M. E. Foster, M. Allendorf and J. Azoulay, *Abstr. Pap. Am. Chem. Soc.*, 2014, **248**, 2081–2090.
- 50 H. A. Lopez, A. Dhakshinamoorthy, B. Ferrer, P. Atienzar, M. Alvaro and H. Garcia, *J. Phys. Chem. C*, 2011, **115**, 22200–22206.
- 51 C. Feng, C. P. Lv, Z. Q. Li, H. Zhao and H. H. Huang, *J. Solid State Chem.*, 2018, **265**, 244–247.
- 52 S. W. Gao, Y. W. Sui, F. X. Wei, J. Q. Qi, Q. K. Meng and Y. Z. He, *J. Mater. Sci.*, 2018, **53**, 6807–6818.
- 53 R. Ramachandran, C. H. Zhao, D. Luo, K. Wang and F. Wang, *Electrochim. Acta*, 2018, **267**, 170–180.
- 54 Y. Jiao, J. Pei, D. H. Chen, C. S. Yan, Y. Y. Hu, Q. Zhang and G. Chen, *J. Mater. Chem. A*, 2017, **5**, 1094–1102.
- 55 N. Ogihara, Y. Ozawa and O. Hiruta, *J. Mater. Chem. A*, 2016, **4**, 3398–3405.
- 56 D. H. Lee, J. H. Ahn, M. S. Park, A. Eftekhari and D. W. Kim, *Electrochim. Acta*, 2018, **283**, 1291–1299.
- 57 Y. Guo, Y. L. Ying, Y. Y. Mao, X. S. Peng and B. L. Chen, *Angew. Chem.-Int. Edit.*, 2016, **55**, 15120–15124.
- 58 S. Y. Bai, X. Z. Liu, K. Zhu, S. C. Wu and H. S. Zhou, *Nat. Energy*, 2016, **1**, 6.
- 59 Z. Z. Yuan, X. X. Zhu, M. R. Li, W. J. Lu, X. F. Li and H. M. Zhang, *Angew. Chem.-Int. Edit.*, 2016, **55**, 3058–3062.

- 60 X. T. Fu, D. N. Yu, J. W. Zhou, S. W. Li, X. Gao, Y. Z. Han, P. F. Qi, X. Feng and B. Wang, *Crystengcomm*, 2016, **18**, 4236-4258.
- 61 J. C. Bachman, S. Muy, A. Grimaud, H. H. Chang, N. Pour, S. F. Lux, O. Paschos, F. Maglia, S. Lupart, P. Lamp, L. Giordano and Y. Shao-Horn, *Chem. Rev.*, 2016, **116**, 140-162.
- 62 M. L. Aubrey, R. Ameloot, B. M. Wiers and J. R. Long, *Energy Environ. Sci.*, 2014, **7**, 667-671.
- 63 Y. Z. Han, P. F. Qi, X. Feng, S. W. Li, X. T. Fu, H. W. Li, Y. F. Chen, J. W. Zhou, X. G. Li and B. Wang, *ACS Appl. Mater. Interfaces*, 2015, **7**, 2178-2182.
- 64 Y. Feng, Y. L. Zhang, G. X. Du, J. B. Zhang and X. H. Qu, *Sustain. Energ. Fuels*, 2018, **2**, 1828-1836.
- 65 X. J. Hong, T. X. Tan, Y. K. Guo, X. Y. Tang, J. Y. Wang, W. Qin and Y. P. Cai, *Nanoscale*, 2018, **10**, 2774-2780.
- 66 H. Zhang, W. Q. Zhao, M. C. Zou, Y. S. Wang, Y. J. Chen, L. Xu, H. S. Wu and A. Y. Cao, *Advanced Energy Materials*, 2018, **8**, 11.
- 67 F. Li, X. M. Zhang, X. B. Liu and M. W. Zhao, *ACS Appl. Mater. Interfaces*, 2018, **10**, 15012-15020.
- 68 X. Z. Zheng, Y. F. Li, Y. X. Xu, Z. S. Hong and M. D. Wei, *Crystengcomm*, 2012, **14**, 2112-2116.
- 69 Z. G. Jiang, T. F. Liu, L. J. Yan, J. Liu, F. F. Dong, M. Ling, C. D. Liang and Z. Lin, *Energy Storage Mater.*, 2018, **11**, 267-273.
- 70 L. N. Nie, J. Xie, G. F. Liu, S. J. Hao, Z. C. J. Xu, R. Xu and Q. C. Zhang, *J. Mater. Chem. A*, 2017, **5**, 17089-17089.
- 71 (a) L. N. Nie, Y. Zhang, K. Q. Ye, J. Y. Han, Y. Wang, G. Rakesh, Y. X. Li, R. Xu, Q. Y. Yan and Q. C. Zhang, *J. Mater. Chem. A*, 2015, **3**, 19410-19416; (b) L. Nie, Y. Zhang, W. Xiong, T.-T. Lim, R. Xu, Q. Yan, Q. Zhang, *Inorg. Chem. Front.*, 2016, **3**, 111-116.
- 72 Y. Y. Ma, J. T. He, Z. K. Kou, A. M. Elshahawy, Y. T. Hu, C. Guan, X. Li and J. Wang, *Adv. Mater. Interfaces*, 2018, **5**, 1800222.
- 73 X. Wang, L. Yu, B. Y. Guan, S. Y. Song and X. W. Lou, *Adv. Mater.*, 2018, **30**, 1801211.
- 74 G. Z. Fang, Z. X. Wu, J. Zhou, C. Y. Zhu, X. X. Cao, T. Q. Lin, Y. M. Chen, C. Wang, A. Q. Pan and S. Q. Liang, *Adv. Energy Mater.*, 2018, **8**, 1703155.
- 75 Y. M. Chen, L. Yu and X. W. Lou, *Angew. Chem.-Int. Edit.*, 2016, **55**, 5990-5993.
- 76 Y. Li, Y. X. Xu, W. P. Yang, W. X. Shen, H. G. Xue and H. Pang, *Small*, 2018, **14**, 1704435.
- 77 X. C. Xie, K. J. Huang and X. Wu, *J. Mater. Chem. A*, 2018, **6**, 6754-6771.
- 78 H. Zhang, X. M. Liu, Y. Wu, C. Guan, A. K. Cheetham and J. Wang, *Chem. Commun.*, 2018, **54**, 5268-5288.
- 79 Q. Ren, H. Wang, X. F. Lu, Y. X. Tong and G. R. Li, *Adv. Sci.*, 2018, **5**, 1700515.
- 80 S. Dang, Q. L. Zhu and Q. Xu, *Nat. Rev. Mater.*, 2018, **3**, 17075.
- 81 D. M. Xu, D. L. Chao, H. W. Wang, Y. S. Gong, R. Wang, B. B. He, X. L. Hu and H. J. Fan, *Adv. Energy Mater.*, 2018, **8**, 1702769.
- 82 C. J. Xuan, B. S. Hou, W. W. Xia, Z. K. Peng, T. Shen, H. L. Xin, G. A. Zhang and D. L. Wang, *J. Mater. Chem. A*, 2018, **6**, 10731-10739.
- 83 J. M. Tarascon and D. Guyomard, *Electrochim. Acta*, 1993, **38**, 1221-1231.
- 84 Y. E. Zhang, S. N. Riduan and J. Q. Wang, *Chem.-Eur. J.*, 2017, **23**, 16419-16431.
- 85 X. X. Li, F. Y. Cheng, S. N. Zhang and J. Chen, *J. Power Sources*, 2006, **160**, 542-547.
- 86 K. Saravanan, M. Nagarathinam, P. Balaya and J. J. Vittal, *J. Mater. Chem.*, 2010, **20**, 8329-8335.
- 87 Y. D. Song, L. L. Yu, Y. Gao, C. D. Shi, M. L. Cheng, X. M. Wang, H. J. Liu and Q. Liu, *Inorg. Chem.*, 2017, **56**, 11603-11609.
- 88 Q. Liu, L. L. Yu, Y. Wang, Y. Z. Ji, J. Horvat, M. L. Cheng, X. Y. Jia and G. X. Wang, *Inorg. Chem.*, 2013, **52**, 2817-2822.
- 89 R. S. Kumar, C. Nithya, S. Gopukumar and M. A. Kulandainathan, *Energy Technol.*, 2014, **2**, 921-927.
- 90 T. C. An, Y. H. Wang, J. Tang, Y. Wang, L. J. Zhang and G. G. Zheng, *J. Colloid Interface Sci.*, 2015, **445**, 320-325.
- 91 C. D. Shi, Y. R. Gao, L. L. Liu, Y. D. Song, X. M. Wang, H. J. Liu and Q. Liu, *J. Nanopart. Res.*, 2016, **18**, 371.
- 92 C. D. Shi, Q. H. Xia, X. Xue, Q. Liu and H. J. Liu, *RSC Adv.*, 2016, **6**, 4442-4447.
- 93 H. W. Song, L. S. Shen, J. Wang and C. X. Wang, *J. Mater. Chem. A*, 2016, **4**, 15411-15419.
- 94 H. W. Liu, H. H. Li, F. Y. Cheng, W. Shi, J. Chen and P. Cheng, *Inorg. Chem.*, 2018, **57**, 10640-10648.
- 95 C. Li, X. S. Hu, X. B. Lou, L. J. Zhang, Y. Wang, J. P. Amoureux, M. Shen, Q. Chen and B. W. Hu, *J. Mater. Chem. A*, 2016, **4**, 16245-16251.
- 96 Y. Luo, L. X. Sun, F. Xu, S. Y. Wei, Q. Y. Wang, H. L. Peng and C. L. Chen, *J. Mater. Sci. Technol.*, 2018, **34**, 1412-1418.
- 97 J. Park, M. Lee, D. W. Feng, Z. H. Huang, A. C. Hinckley, A. Yakovenko, X. D. Zou, Y. Cui and Z. A. Bao, *J. Am. Chem. Soc.*, 2018, **140**, 10315-10323.
- 98 G. Ferey, F. Millange, M. Morcrette, C. Serre, M. L. Doublet, J. M. Greneche and J. M. Tarascon, *Angew. Chem.-Int. Edit.*, 2007, **46**, 3259-3263.
- 99 C. Combettes and M. L. Doublet, *Ionics*, 2008, **14**, 279-283.
- 100 G. de Combarieu, M. Morcrette, F. Millange, N. Guillou, J. Cabana, C. P. Grey, I. Margiolaki, G. Ferey and J. M. Tarascon, *Chem. Mat.*, 2009, **21**, 1602-1611.
- 101 C. Combettes, M. Ben Yahia, L. Pedesseau and M. L. Doublet, *J. Phys. Chem. C*, 2010, **114**, 9518-9527.
- 102 C. Combettes, M. Ben Yahia, L. Pedesseau and M. L. Doublet, *J. Power Sources*, 2011, **196**, 3426-3432.
- 103 J. S. Chavez, K. L. Harrison and D. F. Sava Gallis, *RSC Adv.*, 2017, **7**, 24312-24320.
- 104 J. Shin, M. Kim, J. C. Fernandez, S. Chen, G. Halder, T. Yersak, F. Paesani, S. Cohen and S. Meng, *Abstr. Pap. Am. Chem. Soc.*, 2015, **250**, 4738-4744.
- 105 W. Kaveevivitchai and A. J. Jacobson, *J. Power Sources*, 2015, **278**, 265-273.
- 106 M. Nagarathinam, K. Saravanan, E. J. H. Phua, M. V. Reddy, B. V. R. Chowdari and J. J. Vittal, *Angew. Chem.-Int. Edit.*, 2012, **51**, 5866-5870.
- 107 A. S. Hameed, M. Nagarathinam, M. Schreyer, M. V. Reddy, B. V. R. Chowdari and J. J. Vittal, *J. Mater. Chem. A*, 2013, **1**, 5721-5726.
- 108 Q. H. Wang, Q. X. Wang, B. Y. Xu, F. Gao, F. Gao and C. Zhao, *Electrochim. Acta*, 2018, **281**, 69-77.
- 109 Q. M. Gan, H. N. He, K. M. Zhao, Z. He and S. Q. Liu, *J. Colloid Interface Sci.*, 2018, **530**, 127-136.
- 110 X. M. Sun, G. Gao, D. W. Yan and C. Q. Feng, *Appl. Surf. Sci.*, 2017, **405**, 52-59.
- 111 S. Maiti, A. Pramanik, U. Manju and S. Mahanty, *Microporous Mesoporous Mat.*, 2016, **226**, 353-359.
- 112 S. Maiti, A. Pramanik, U. Manju and S. Mahanty, *ACS Appl. Mater. Interfaces*, 2015, **7**, 16357-16363.
- 113 L. Chen, W. J. Yang, J. B. Wang, C. R. Chen and M. D. Wei, *Chem.-Eur. J.*, 2018, **24**, 13362-13367.
- 114 X. S. Hu, H. P. Hu, C. Li, T. Li, X. B. Lou, Q. Chen and B. W. Hu, *J. Solid State Chem.*, 2016, **242**, 71-76.
- 115 L. Gou, L. M. Hao, Y. X. Shi, S. L. Ma, X. Y. Fan, L. Xu, D. L. Li and K. Wang, *J. Solid State Chem.*, 2014, **210**, 121-124.
- 116 Y. Luo, L. X. Sun, F. Xu, S. Y. Wei, Q. Y. Wang, H. L. Peng and C. L. Chen, *J. Mater. Sci. Technol.*, 2018, **34**, 1412-1418.
- 117 Y. X. Liao, C. Li, X. B. Lou, P. Wang, Q. Yang, M. Shen and B. W. Hu, *J. Colloid Interface Sci.*, 2017, **506**, 365-372.
- 118 L. Gou, P. G. Liu, H. Y. Lei, G. Q. Chen, Z. Y. Li, X. Y. Fan, D. L. Li and L. F. Song, *Mater. Technol.*, 2017, **32**, 630-637.

- 119 L. Gou, L. Ma, M. J. Zhao, P. G. Liu, X. D. Wang, X. Y. Fan and D. L. Li, *J. Mater. Sci.*, 2019, **54**, 1529-1538.
- 120 F. Yang, W. Y. Li, Y. F. Zhang and B. H. J. Tang, *Dalton Trans.*, 2018, **47**, 13657-13667.
- 121 P. Wang, X. B. Lou, C. Li, X. S. Hu, Q. Yang and B. W. Hu, *Nano-Micro Lett.*, 2018, **10**, 19.
- 122 Y. C. Lin, Q. J. Zhang, C. C. Zhao, H. L. Li, C. L. Kong, C. Shen and L. Chen, *Chem. Commun.*, 2015, **51**, 697-699.
- 123 Z. Li, X. X. Huang, C. L. Sun, X. Y. Chen, J. B. Hu, A. Stein and B. H. J. Tang, *J. Mater. Sci.*, 2017, **52**, 3979-3991.
- 124 C. Li, Q. Yang, M. Shen, J. Y. Ma and B. W. Hu, *Energy Storage Mater.*, 2018, **14**, 82-89.
- 125 Y. Q. Ning, X. B. Lou, C. Li, X. S. Hu and B. W. Hu, *Chem.-Eur. J.*, 2017, **23**, 15984-15990.
- 126 X. S. Hu, X. B. Lou, C. Li, Y. Q. Ning, Y. X. Liao, Q. Chen, E. S. Mananga, M. Shen and B. W. Hu, *RSC Adv.*, 2016, **6**, 114483-114490.
- 127 C. H. Zhang, W. Q. Hu, H. Jiang, J. K. Chang, M. S. Zheng, Q. H. Wu and Q. F. Dong, *Electrochim. Acta*, 2017, **246**, 528-535.
- 128 Z. Peng, X. H. Yi, Z. X. Liu, J. Shang and D. Y. Wang, *ACS Appl. Mater. Interfaces*, 2016, **8**, 14578-14585.
- 129 Z. Y. Zhang, H. Yoshikawa and K. Awaga, *J. Am. Chem. Soc.*, 2014, **136**, 16112-16115.
- 130 X. Y. Han, F. Yi, T. L. Sun and J. T. Sun, *Electrochem. Commun.*, 2012, **25**, 136-139.
- 131 T. L. Nguyen, T. Devic, P. Mialane, E. Riviere, A. Sonnauer, N. Stock, R. Demir-Cakan, M. Morcrette, C. Livage, J. Marrot, J. M. Tarascon and G. Ferey, *Inorg. Chem.*, 2010, **49**, 10710-10717.
- 132 K. Wada, K. Sakaushi, S. Sasaki and H. Nishihara, *Angew. Chem.-Int. Edit.*, 2018, **57**, 8886-8890.
- 133 Z. Y. Zhang, H. Yoshikawa and K. Awaga, *Chem. Mat.*, 2016, **28**, 1298-1303.
- 134 C. F. Dong and L. Q. Xu, *ACS Appl. Mater. Interfaces*, 2017, **9**, 7160-7168.
- 135 H. P. Hu, X. B. Lou, C. Li, X. S. Hu, T. Li, Q. Chen, M. Shen and B. W. Hu, *New J. Chem.*, 2016, **40**, 9746-9752.
- 136 C. D. Shi, X. M. Wang, Y. R. Gao, H. R. Rong, Y. D. Song, H. J. Liu and Q. Liu, *J. Solid State Electr.*, 2017, **21**, 2415-2423.
- 137 L. Hu, X. M. Lin, J. T. Mo, J. Lin, H. L. Gan, X. L. Yang and Y. P. Cai, *Inorg. Chem.*, 2017, **56**, 4289-4295.
- 138 M. Schleep, S. Reininger, P. Eiden, P. Klose, C. Schulz, H. Scherer, S. Laule, S. Bodendorfer, M. Schmidt, A. Garsuch and I. Krossing, *Chemelectrochem*, 2016, **3**, 774-782.
- 139 L. Hu, X. M. Lin, J. Lin, R. Q. Zhang, D. L. Zhang and Y. P. Cai, *Crystengcomm*, 2016, **18**, 9307-9315.
- 140 Y. Wang, Q. T. Qu, G. Liu, V. S. Battaglia and H. H. Zheng, *Nano Energy*, 2017, **39**, 200-210.
- 141 S. S. Zheng, X. R. Li, B. Y. Yan, Q. Hu, Y. X. Xu, X. Xiao, H. G. Xue and H. Pang, *Adv. Energy Mater.*, 2017, **7**, 1602733.
- 142 J. F. Xiang, C. X. Chang, M. Li, S. M. Wu, L. J. Yuan and J. T. Sun, *Cryst. Growth Des.*, 2008, **8**, 280-282.
- 143 T. L. A. Nguyen, R. Demir-Cakan, T. Devic, M. Morcrette, T. Ahnfeldt, P. Auban-Senzier, N. Stock, A. M. Goncalves, Y. Filinchuk, J. M. Tarascon and G. Ferey, *Inorg. Chem.*, 2010, **49**, 7135-7143.
- 144 P. C. Cheng, F. S. Tseng, C. T. Yeh, T. G. Chang, C. C. Kao, C. H. Lin, W. R. Liu, J. S. Chen and V. Zima, *Crystengcomm*, 2012, **14**, 6812-6822.
- 145 C. D. Malliakas, K. Leung, K. Z. Pupek, I. A. Shkrob and D. P. Abraham, *Phys. Chem. Chem. Phys.*, 2016, **18**, 10846-10849.
- 146 B. F. Abrahams, M. J. Grannas, T. A. Hudson and R. Robson, *Angew. Chem.-Int. Edit.*, 2010, **49**, 1087-1089.
- 147 S. Tominaka, H. H. M. Yeung, S. Henke and A. K. Cheetham, *Crystengcomm*, 2016, **18**, 398-406.
- 148 T. Wei, M. Zhang, P. Wu, Y. J. Tang, S. L. Li, F. C. Shen, X. L. Wang, X. P. Zhou and Y. Q. Lan, *Nano Energy*, 2017, **34**, 205-214.
- 149 Q. Huang, T. Wei, M. Zhang, L. Z. Dong, A. M. Zhang, S. L. Li, W. J. Liu, J. Liu and Y. Q. Lan, *J. Mater. Chem. A*, 2017, **5**, 8477-8483.
- 150 X. Y. Yang, T. Wei, J. S. Li, N. Sheng, P. P. Zhu, J. Q. Sha, T. Wang and Y. Q. Lan, *Inorg. Chem.*, 2017, **56**, 8311-8318.
- 151 Y. Y. Wang, M. Zhang, S. L. Li, S. R. Zhang, W. Xie, J. S. Qin, Z. M. Su and Y. Q. Lan, *Chem. Commun.*, 2017, **53**, 5204-5207.
- 152 Y. C. He, N. Xu, Y. Yu, X. L. Geng, W. Q. Kan, Q. Chen and J. M. You, *Polyhedron*, 2017, **137**, 278-283.
- 153 Y. F. Yue, Y. C. Li, Z. H. Bi, G. M. Veith, C. A. Bridges, B. K. Guo, J. H. Chen, D. R. Mullins, S. P. Surwade, S. M. Mahurin, H. J. Liu, M. P. Paranthaman and S. Dai, *J. Mater. Chem. A*, 2015, **3**, 22989-22995.
- 154 S. Z. Ji, J. Y. Zhang, W. W. Wang, Y. Huang, Z. R. Feng, Z. T. Zhang and Z. L. Tang, *Mater. Chem. Phys.*, 2010, **123**, 510-515.
- 155 Y. L. Wang, X. Huang, F. Li, J. S. Cao and S. H. Ye, *RSC Adv.*, 2015, **5**, 49651-49656.
- 156 C. Li, X. S. Hu, X. B. Lou, Q. Chen and B. W. Hu, *Chem. Commun.*, 2016, **52**, 2035-2038.
- 157 S. B. Kim, J. Y. Kim, N. C. Jeong and K. M. Ok, *Inorg. Chem. Front.*, 2017, **4**, 79-83.
- 158 J. P. Tan, F. N. Shi, F. Hu, G. M. Shi, B. Tian and H. P. You, *Inorg. Chem. Commun.*, 2018, **91**, 112-118.
- 159 X. B. Lou, Y. Q. Ning, C. Li, X. S. Hu, M. Shen and B. W. Hu, *Sci. China Mater.*, 2018, **61**, 1040-1048.
- 160 Y. X. Chen, D. Ni, X. W. Yang, C. C. Liu, J. L. Yin and K. F. Cai, *Electrochim. Acta*, 2018, **278**, 114-123.
- 161 T. Li, C. Li, X. S. Hu, X. B. Lou, H. P. Hu, L. K. Pan, Q. Chen, M. Shen and B. W. Hu, *RSC Adv.*, 2016, **6**, 61319-61324.
- 162 M. A. Oliver-Tolentino, J. Vazquez-Samperio, R. Cabrera-Sierra and E. Reguer, *RSC Adv.*, 2016, **6**, 108627-108634.
- 163 C. Li, X. B. Lou, Q. Yang, Y. M. Zou and B. W. Hu, *Chem. Eng. J.*, 2017, **326**, 1000-1008.
- 164 T. Kambe, R. Sakamoto, K. Hoshiko, K. Takada, M. Miyachi, J. H. Ryu, S. Sasaki, J. Kim, K. Nakazato, M. Takata and H. Nishihara, *J. Am. Chem. Soc.*, 2013, **135**, 2462-2465.
- 165 A. Fateeva, P. Horcajada, T. Devic, C. Serre, J. Marrot, J. M. Greneche, M. Morcrette, J. M. Tarascon, G. Maurin and G. Ferey, *Eur. J. Inorg. Chem.*, 2010, **2010**, 3789-3794.
- 166 J. Shin, M. Kim, J. Cirera, S. Chen, G. J. Halder, T. A. Yersak, F. Paesani, S. M. Cohen and Y. S. Meng, *J. Mater. Chem. A*, 2015, **3**, 4738-4744.
- 167 L. S. Shen, H. W. Song and C. X. Wang, *Electrochim. Acta*, 2017, **235**, 595-603.
- 168 C. Li, X. S. Hu and B. W. Hu, *Electrochim. Acta*, 2017, **253**, 439-444.
- 169 B. H. J. Tang, S. P. Huang, Y. Fang, J. B. Hu, C. Malonzo, D. G. Truhlar and A. Stein, *J. Chem. Phys.*, 2016, **144**, 194702.
- 170 D. F. Sava Gallis, H. D. Pratt, T. M. Anderson and K. W. Chapman, *J. Mater. Chem. A*, 2016, **4**, 13764-13770.
- 171 C. Li, X. B. Lou, M. Shen, X. S. Hu, Z. Guo, Y. Wang, B. W. Hu and Q. Chen, *ACS Appl. Mater. Interfaces*, 2016, **8**, 15352-15360.
- 172 H. L. Fei, W. J. Feng and T. Xu, *J. Colloid Interface Sci.*, 2017, **488**, 277-281.
- 173 T. Yasuda and N. Ogihara, *Chem. Commun.*, 2014, **50**, 11565-11567.
- 174 M. L. Aubrey and J. R. Long, *J. Am. Chem. Soc.*, 2015, **137**, 13594-13602.
- 175 H. L. Fei, X. Liu and Z. W. Li, *Chem. Eng. J.*, 2015, **281**, 453-458.
- 176 L. Gou, P. G. Liu, D. Liu, C. Y. Wang, H. Y. Lei, Z. Y. Li, X. Y. Fan and D. L. Li, *Dalton Trans.*, 2017, **46**, 6473-6482.
- 177 C. C. Zhao, C. Shen and W. Q. Han, *RSC Adv.*, 2015, **5**, 20386-20389.
- 178 L. Zhang, F. Y. Cheng, W. Shi, J. Chen and P. Cheng, *ACS Appl. Mater. Interfaces*, 2018, **10**, 6398-6406.

- 179 H. J. Kim, Y. Kim, J. Shim, K. H. Jung, M. S. Jung, H. Kim, J. C. Lee and K. T. Lee, *ACS Appl. Mater. Interfaces*, 2018, **10**, 3479-3486.
- 180 C. Fang, Y. Huang, L. X. Yuan, Y. J. Liu, W. L. Chen, Y. Y. Huang, K. Y. Chen, J. T. Han, Q. J. Liu and Y. H. Huang, *Angew. Chem.-Int. Edit.*, 2017, **56**, 6793-6797.
- 181 L. Sun, J. Xie, Z. D. Chen, J. Wu and L. Li, *Dalton Trans.*, 2018, **47**, 9989-9993.
- 182 X. Huang, P. Sheng, Z. Y. Tu, F. J. Zhang, J. H. Wang, H. Geng, Y. Zou, C. A. Di, Y. P. Yi, Y. M. Sun, W. Xu and D. B. Zhu, *Nat. Commun.*, 2015, **6**, 7408.
- 183 H. L. Fei, Y. Q. Lin and T. Xu, *Ionics*, 2017, **23**, 1949-1954.
- 184 H. L. Fei and Y. Q. Lin, *J. Colloid Interface Sci.*, 2016, **481**, 256-262.
- 185 H. L. Fei, X. Liu, Z. W. Li and W. J. Feng, *Dalton Trans.*, 2015, **44**, 9909-9914.
- 186 G. H. Li, H. Yang, F. C. Li, F. Y. Cheng, W. Shi, J. Chen and P. Cheng, *Inorg. Chem.*, 2016, **55**, 4935-4940.
- 187 C. Li, X. B. Lou, M. Shen, X. S. Hu, W. S. Yan, Y. M. Zou, W. Tong and B. W. Hu, *Energy Storage Mater.*, 2017, **7**, 195-202.
- 188 X. B. Lou, X. S. Hu, C. Li, Y. Q. Ning, Q. Chen, M. Shen and B. W. Hu, *New J. Chem.*, 2017, **41**, 1813-1819.
- 189 L. L. Yu, X. M. Wang, M. L. Cheng, H. R. Rong, Y. D. Song and Q. Liu, *Cryst. Growth Des.*, 2018, **18**, 280-285.
- 190 T. Gong, X. B. Lou, J. J. Fang, E. Q. Gao and B. W. Hu, *Dalton Trans.*, 2016, **45**, 19109-19116.
- 191 H. L. Fei, X. Liu, Z. W. Li and W. J. Feng, *Electrochim. Acta*, 2015, **174**, 1088-1095.
- 192 Y. Q. Ning, X. B. Lou, M. Shen and B. W. Hu, *Mater. Lett.*, 2017, **197**, 245-248.
- 193 H. H. Lee, J. B. Lee, Y. Park, K. H. Park, M. S. Okyay, D. S. Shin, S. Kim, J. Park, N. Park, B. K. An, Y. S. Jung, H. W. Lee, K. T. Lee and S. Y. Hong, *ACS Appl. Mater. Interfaces*, 2018, **10**, 22110-22118.
- 194 B. B. Tian, G. H. Ning, Q. Gao, L. M. Tan, W. Tang, Z. X. Chen, C. L. Su and K. P. Loh, *ACS Appl. Mater. Interfaces*, 2016, **8**, 31067-31075.
- 195 T. Gong, X. B. Lou, E. Q. Gao and B. W. Hu, *ACS Appl. Mater. Interfaces*, 2017, **9**, 21839-21847.
- 196 M. Cognet, T. Gutel, D. Peralta, J. Maynadie, M. Carboni and D. Meyer, *J. Electrochem. Soc.*, 2017, **164**, A2552-A2554.
- 197 N. Lahiri, N. Lotfizadeh, R. Tsuchikawa, V. V. Deshpande and J. Louie, *J. Am. Chem. Soc.*, 2017, **139**, 2119-2119.
- 198 J. H. Dou, L. Sun, Y. C. Ge, W. Li, C. H. Hendon, J. Li, S. Gul, J. K. Yano, E. A. Stach and M. Dinca, *J. Am. Chem. Soc.*, 2017, **139**, 13608-13611.
- 199 D. W. Feng, T. Lei, M. R. Lukatskaya, J. Park, Z. H. Huang, M. Lee, L. Shaw, S. C. Chen, A. A. Yakovenko, A. Kulkarni, J. P. Xiao, K. Fredrickson, J. B. Tok, X. D. Zou, Y. Cui and Z. A. Bao, *Nat. Energy*, 2018, **3**, 30-36.
- 200 G. P. Gao, F. Zheng, F. Pan and L. W. Wang, *Adv. Energy Mater.*, 2018, **8**, 1801823.
- 201 T. Kambe, R. Sakamoto, T. Kusamoto, T. Pal, N. Fukui, K. Hoshiko, T. Shimojima, Z. F. Wang, T. Hirahara, K. Ishizaka, S. Hasegawa, F. Liu and H. Nishihara, *J. Am. Chem. Soc.*, 2014, **136**, 14357-14360.
- 202 X. Huang, H. Y. Yao, Y. T. Cui, W. Hao, J. Zhu, W. Xu and D. B. Zhu, *ACS Appl. Mater. Interfaces*, 2017, **9**, 40752-40759.
- 203 X. Huang, S. Zhang, L. Y. Liu, L. Yu, G. F. Chen, W. Xu and D. B. Zhu, *Angew. Chem.-Int. Edit.*, 2018, **57**, 146-150.
- 204 X. Huang, H. Li, Z. Tu, L. Liu, X. Wu, J. Chen, Y. Liang, Y. Zou, Y. Yi and J. Sun, *J. Am. Chem. Soc.*, 2018, **45**, 15153-15156.
- 205 X. M. Zhang, Y. N. Zhou, B. Cui, M. W. Zhao and F. Liu, *Nano Letters*, 2017, **17**, 6166-6170.
- 206 S. W. Kim, D. H. Seo, X. H. Ma, G. Ceder and K. Kang, *Adv. Energy Mater.*, 2012, **2**, 710-721.
- 207 S. H. He, Z. P. Li, L. M. Ma, J. Q. Wang and S. R. Yang, *New J. Chem.*, 2017, **41**, 14209-14216.
- 208 S. Ghasemi, S. R. Hosseini and P. Asen, *Electrochim. Acta*, 2015, **160**, 337-346.
- 209 Y. Jin, C. C. Zhao, Z. X. Sun, Y. C. Lin, L. Chen, D. Y. Wang and C. Shen, *RSC Adv.*, 2016, **6**, 30763-30768.
- 210 B. Le Ouay, M. Boudot, T. Kitao, T. Yanagida, S. Kitagawa and T. Uemura, *J. Am. Chem. Soc.*, 2016, **138**, 10088-10091.
- 211 Y. Jiao, G. Chen, D. H. Chen, J. Pei and Y. Y. Hu, *J. Mater. Chem. A*, 2017, **5**, 23744-23752.
- 212 P. T. Xiao, F. X. Bu, R. R. Zhao, M. F. A. Aboud, I. Shakir and Y. X. Xu, *ACS Nano*, 2018, **12**, 3947-3953.
- 213 W. Y. Li, F. Yang, X. J. Fang, Y. C. Rui and B. J. Tang, *Electrochim. Acta*, 2018, **282**, 276-285.
- 214 R. S. Potember, R. C. Hoffman, H. S. Hu, J. E. Cocchiario, C. A. Viands, R. A. Murphy and T. O. Poehler, *Polymer*, 1987, **28**, 574-580.
- 215 L. Sun, M. G. Campbell and M. Dinca, *Angew. Chem.-Int. Edit.*, 2016, **55**, 3566-3579.
- 216 C. F. Leong, P. M. Usov and D. M. D'Alessandro, *Mrs Bull.*, 2016, **41**, 858-864.
- 217 E. A. Dolgoplova, A. J. Brandt, O. A. Ejegbavwo, A. S. Duke, T. D. Maddumapatabandi, R. P. Galhenage, B. W. Larson, O. G. Reid, S. C. Ammal, A. Heyden, M. Chandrashekar, V. Stavila, D. A. Chen and N. B. Shustova, *J. Am. Chem. Soc.*, 2017, **139**, 5201-5209.
- 218 S. Sundriyal, H. Kaur, S. K. Bhardwaj, S. Mishra, K. H. Kim and A. Deep, *Coord. Chem. Rev.*, 2018, **369**, 15-38.
- 219 D. Sheberla, J. C. Bachman, J. S. Elias, C. J. Sun, Y. Shao-Horn and M. Dinca, *Nat. Mater.*, 2017, **16**, 220-224.
- 220 N. Ogihara, N. Ohba and Y. Kishida, *Sci. Adv.*, 2017, **3**, e1603103.
- 221 N. Ogihara, T. Yasuda, Y. Kishida, T. Ohsuna, K. Miyamoto and N. Ohba, *Angew. Chem.-Int. Edit.*, 2014, **53**, 11467-11472.
- 222 C. Y. Cheng, S. J. Fu, C. J. Yang, W. H. Chen, K. J. Lin, G. H. Lee and Y. Wang, *Angew. Chem.-Int. Edit.*, 2003, **42**, 1937-1940.
- 223 T. Yamada, K. Shiraishi, H. Kitagawa and N. Mizumoto, *Chem. Commun.*, 2017, **53**, 8215-8218.
- 224 T. Shimizu, H. Wang, N. Tanifuji, D. Matsumura, M. Yoshimura, K. Nakanishi, T. Ohta and H. Yoshikawa, *Chem. Lett.*, 2018, **47**, 678-681.
- 225 A. Paoletta, C. Faure, V. Timoshevskii, S. Marras, G. Bertoni, A. Guerfi, A. Vijh, M. Armand and K. Zaghib, *J. Mater. Chem. A*, 2017, **5**, 18919-18932.
- 226 J. Nai and X. W. Lou, *Adv. Mater.*, 2018, 1706825.
- 227 J. Qian, C. Wu, Y. Cao, Z. Ma, Y. Huang, X. Ai and H. Yang, *Adv. Energy Mater.*, 2018, 1702619.
- 228 L. Catala and T. Mallah, *Coord. Chem. Rev.*, 2017, **346**, 32-61.
- 229 F. Ma, Q. Li, T. Wang, H. Zhang and G. Wu, *Sci. Bull.*, 2017, **62**, 358-368.
- 230 Y. H. Lu, L. Wang, J. G. Cheng and J. B. Goodenough, *Chem. Commun.*, 2012, **48**, 6544-6546.
- 231 W. H. Ren, M. S. Qin, Z. X. Zhu, M. Y. Yan, Q. Li, L. Zhang, D. N. Liu and L. Q. Mai, *Nano Lett.*, 2017, **17**, 4713-4718.
- 232 V. D. Neff, *J. Electrochem. Soc.*, 1985, **132**, 1382-1384.
- 233 M. Kaneko, *J. Polym. Sci. Pol. Lett.*, 1986, **24**, 435-437.
- 234 M. Kaneko and T. Okada, *J. Electroanal. Chem.*, 1988, **255**, 45-52.
- 235 L. Wang, Y. H. Lu, J. Liu, M. W. Xu, J. G. Cheng, D. W. Zhang and J. B. Goodenough, *Angew. Chem.-Int. Edit.*, 2013, **52**, 1964-1967.
- 236 Y. You, X. L. Wu, Y. X. Yin and Y. G. Guo, *Energy Environ. Sci.*, 2014, **7**, 1643-1647.
- 237 H. W. Lee, R. Y. Wang, M. Pasta, S. W. Lee, N. Liu and Y. Cui, *Nat. Commun.*, 2014, **5**, 5280.
- 238 Y. Liu, Y. Qiao, W. X. Zhang, Z. Li, X. Ji, L. Miao, L. X. Yuan, X. L. Hu and Y. H. Huang, *Nano Energy*, 2015, **12**, 386-393.
- 239 X. F. Bie, K. Kubota, T. Hosaka, K. Chihara and S. Komaba, *J. Power Sources*, 2018, **378**, 322-330.

- 240 C. Li, R. Zang, P. X. Li, Z. M. Man, S. J. Wang, X. M. Li, Y. H. Wu, S. S. Liu and G. X. Wang, *Chem-Asian J.*, 2018, **13**, 342-349.
- 241 H. Fu, C. Liu, C. Zhang, W. Ma, K. Wang, Z. Li, X. Lu and G. Cao, *J. Mater. Chem. A*, 2017, **5**, 9604-9610.
- 242 P. Marzak, J. Yun, A. Dorsel, A. Kriele, R. Gilles, O. Schneider and A. S. Bandarenka, *J. Phys. Chem. C*, 2018, **122**, 8760-8768.
- 243 H. Sun, W. Zhang and M. Hu, *Crystals*, 2018, **8**, 23.
- 244 J. H. Lee, G. Ali, D. H. Kim and K. Y. Chung, *Adv. Energy Mater.*, 2017, **7**, 1601491.
- 245 B. Paulitsch, J. Yun and A. S. Bandarenka, *ACS Appl. Mater. Interfaces*, 2017, **9**, 8107-8112.
- 246 L. Zhou, Z. K. Yang, C. Y. Li, B. W. Chen, Y. F. Wang, L. J. Fu, Y. S. Zhu, X. Liu and Y. P. Wu, *RSC Adv.*, 2016, **6**, 109340-109345.
- 247 C. D. Wessells, R. A. Huggins and Y. Cui, *Nat. Commun.*, 2011, **2**, 550.
- 248 J. Peng, J. Wang, H. Yi, W. Hu, Y. Yu, J. Yin, Y. Shen, Y. Liu, J. Luo and Y. Xu, *Adv. Energy Mater.*, 2018, **8**, 1702856.
- 249 W. H. Ren, M. S. Qin, Z. X. Zhu, M. Y. Yan, Q. Li, L. Zhang, D. N. Liu and L. Q. Mai, *Nano Letters*, 2017, **17**, 4713-4718.
- 250 D. S. Kim, M. B. Zakaria, M. S. Park, A. Alowasheir, S. M. Alshehri, Y. Yamauchi and H. Kim, *Electrochim. Acta*, 2017, **240**, 300-306.
- 251 Y. Liu, G. Y. Wei, M. Y. Ma and Y. Qiao, *Chem.-Eur. J.*, 2017, **23**, 15991-15996.
- 252 X. Tang, H. Liu, D. W. Su, P. H. L. Notten and G. X. Wang, *Nano Res.*, 2018, **11**, 3979-3990.
- 253 Y. X. Huang, M. Xie, J. T. Zhang, Z. H. Wang, Y. Jiang, G. H. Xiao, S. J. Li, L. Li, F. Wu and R. J. Chen, *Nano Energy*, 2017, **39**, 273-283.
- 254 Y. F. Yue, A. J. Binder, B. K. Guo, Z. Y. Zhang, Z. A. Qiao, C. C. Tian and S. Dai, *Angew. Chem.-Int. Edit.*, 2014, **53**, 3134-3137.
- 255 C. H. Li, Y. Nanba, D. Asakura, M. Okubo and D. R. Talham, *RSC Adv.*, 2014, **4**, 24955-24961.
- 256 Y. You, H. R. Yao, S. Xin, Y. X. Yin, T. T. Zuo, C. P. Yang, Y. G. Guo, Y. Cui, L. J. Wan and J. B. Goodenough, *Adv. Mater.*, 2016, **28**, 7243-7248.
- 257 N. Imanishi, T. Morikawa, J. Kondo, Y. Takeda, O. Yamamoto, N. Kinugasa and T. Yamagishi, *J. Power Sources*, 1999, **79**, 215-219.
- 258 X. Y. Wu, M. M. Shao, C. H. Wu, J. F. Qian, Y. L. Cao, X. P. Ai and H. X. Yang, *ACS Appl. Mater. Interfaces*, 2016, **8**, 23706-23712.
- 259 J. Long, D. Asakura, M. Okubo, A. Yamada, Y. Guari and J. Larionova, *Inorg. Chem.*, 2016, **55**, 7637-7646.
- 260 S. Yagi, M. Fukuda, R. Makiura, T. Ichitsubo and E. Matsubara, *J. Mater. Chem. A*, 2014, **2**, 8041-8047.
- 261 C. H. Li, M. K. Peprah, D. Asakura, M. W. Meisel, M. Okubo and D. R. Talham, *Chem. Mat.*, 2015, **27**, 1524-1530.
- 262 M. Z. Zhu, H. Zhou, J. X. Shao, J. H. Feng and A. H. Yuan, *J. Alloy Compd.*, 2018, **749**, 811-817.
- 263 L. Zhang, T. Meng, B. G. Mao, D. L. Guo, J. W. Qin and M. H. Cao, *RSC Adv.*, 2017, **7**, 50812-50821.
- 264 T. Shibata, M. Takachi and Y. Moritomo, *Batteries*, 2017, **3**, 7.
- 265 P. Nie, L. F. Shen, H. F. Luo, B. Ding, G. Y. Xu, J. Wang and X. G. Zhang, *J. Mater. Chem. A*, 2014, **2**, 5852-5857.
- 266 A. Fateeva, P. Horcjada, T. Devic, C. Serre, J. Marrot, J. M. Greneche, M. Morcrette, J. M. Tarascon, G. Maurin and G. Ferey, *Eur. J. Inorg. Chem.*, 2010, 3789-3794.
- 267 B. W. Qin, K. C. Huang, Y. Zhang, L. Zhou, Z. Cui, K. Zhang, X. Y. Zhang and J. P. Zhang, *Chem.-Eur. J.*, 2018, **24**, 1962-1970.
- 268 N. Phattharasupakun, J. Wutthiprom, S. Kaenket, T. Maihom, J. Limtrakul, M. Probst, S. S. Nagarkar, S. Horike and M. Sawangphruk, *Chem. Commun.*, 2017, **53**, 11786-11789.
- 269 M. Zhao, Q. Lu, Q. Ma and H. Zhang, *Small Methods*, 2017, **1**, 1600030.
- 270 P. Kumar, K. H. Kim, V. Bansal and P. Kumar, *Coord. Chem. Rev.*, 2017, **353**, 113-141.
- 271 M. Cognet, T. Gutel, R. Gautier, X. F. Le Goff, A. Mesbah, N. Dacheux, M. Carboni and D. Meyer, *Materials Letters*, 2019, **236**, 73-76.
- 272 Y. Zhu, S. Wang, Z. Miao, Y. Liu and S. L. Chou, *Small*, 2018, **14**, 1801987.
- 273 H. Jiang, X. C. Liu, Y. Wu, Y. Shu, X. Gong, F. S. Ke and H. Deng, *Angew. Chem. Int. Ed.*, 2018, **130**, 3980-3985.
- 274 J. Xu, T. Lawson, H. Fan, D. Su and G. Wang, *Adv. Energy Mater.*, 2018, **8**, 1702607.
- 275 Y. Zhao, J. Liu, M. Horn, N. Motta, M. Hu and Y. Li, *Sci. China Mater.*, 2018, **61**, 159-184.
- 276 K. Zhao, S. Liu, G. Ye, Q. Gan, Z. Zhou and Z. He, *J. Mater. Chem. A*, 2018, **6**, 2166-2175.
- 277 D. P. Dubal, N. R. Chodankar, D.-H. Kim and P. Gomez-Romero, *Chem. Soc. Rev.*, 2018, **47**, 2065-2129.
- 278 H. Li, J. Lang, S. Lei, J. Chen, K. Wang, L. Liu, T. Zhang, W. Liu and X. Yan, *Adv. Funct. Mater.*, 2018, **28**, 1800757.
- 279 D. Wu, Z. Guo, X. Yin, Q. Pang, B. Tu, L. Zhang, Y. G. Wang and Q. Li, *Adv. Mater.*, 2014, **26**, 3258-3262.
- 280 X. Hu, Z. Zhu, F. Cheng, Z. Tao and J. Chen, *Nanoscale*, 2015, **7**, 11833-11840.
- 281 Z. Shadike, D.-R. Shi, M.-H. Cao, S.-F. Yang, J. Chen and Z.-W. Fu, *J. Mater. Chem. A*, 2017, **5**, 6393-6398.
- 282 X. Bie, K. Kubota, T. Hosaka, K. Chihara and S. Komaba, *J. Mater. Chem. A*, 2017, **5**, 4325-4330.
- 283 C. Li, X. Hu and B. Hu, *Electrochim. Acta*, 2017, **253**, 439-444.
- 284 X. Wu, Z. Jian, Z. Li and X. Ji, *Electrochem. Commun.*, 2017, **77**, 54-57.
- 285 X. Wu, D. P. Leonard and X. Ji, *Chem. Mat.*, 2017, **29**, 5031-5042.
- 286 G. He and L. F. Nazar, *ACS Energy Lett.*, 2017, **2**, 1122-1127.
- 287 A. Eftekhari, *J. Power Sources*, 2004, **136**, 201-201.
- 288 L. Zhou, M. Zhang, Y. Wang, Y. Zhu, L. Fu, X. Liu, Y. Wu and W. Huang, *Electrochim. Acta*, 2017, **232**, 106-113.
- 289 A. Baïoun, H. Kellawi and A. Falah, *Curr. Nanosci.*, 2018, **14**, 227-233.
- 290 L. Deng, Z. Yang, L. Tan, L. Zeng, Y. Zhu and L. Guo, *Adv. Mater.*, 2018, 1802510.
- 291 L. Xue, Y. Li, H. Gao, W. Zhou, X. Lu, W. Kaveevivitchai, A. Manthiram and J. B. Goodenough, *J. Am. Chem. Soc.*, 2017, **139**, 2164-2167.
- 292 S. S. Park, Y. Tulchinsky and M. Dinca, *J. Am. Chem. Soc.*, 2017, **139**, 13260-13263.
- 293 H. Zhang, Y. Yu, L. L. Zhang, Y. W. Zhai and S. J. Dong, *Chem. Sci.*, 2016, **7**, 6721-6727.
- 294 R. Y. Wang, B. Shyam, K. H. Stone, J. N. Weker, M. Pasta, H. W. Lee, M. F. Toney and Y. Cui, *Adv. Energy Mater.*, 2015, **5**, 1401869.
- 295 Y. Mizuno, M. Okubo, E. Hosono, T. Kudo, K. Oh-ishi, A. Okazawa, N. Kojima, R. Kuroono, S. Nishimura and A. Yamada, *J. Mater. Chem. A*, 2013, **1**, 13055-13059.
- 296 L. Chen, J. L. Bao, X. Dong, D. G. Truhlar, Y. Wang, C. Wang and Y. Xia, *ACS Energy Lett.*, 2017, **2**, 1115-1121.
- 297 M. S. Chae, J. W. Heo, H. H. Kwak, H. Lee and S. T. Hong, *J. Power Sources*, 2017, **337**, 204-211.
- 298 Q. D. Truong, M. K. Devaraju, D. N. Nguyen, Y. Gambe, K. Nayuki, Y. Sasaki, P. D. Tran and I. Honma, *Nano Lett.*, 2016, **16**, 5829-5835.